UNIVERSIDADE FEDERAL DO RIO GRANDE DO SUL

INSTITUTO DE PESQUISAS HIDRÁULICAS

PROGRAMA DE PÓS-GRADUAÇÃO EM RECURSOS HÍDRICOS E SANEAMENTO AMBIENTAL

Rafael Barbedo Fontana

IDENTIFYING AND ASSESSING VEGETATION BEHAVIOUR IN RIPARIAN ZONES AT LARGE SCALE IN THE BRAZILIAN SAVANNAH

PORTO ALEGRE

2020

Rafael Barbedo Fontana

IDENTIFYING AND ASSESSING VEGETATION BEHAVIOUR IN RIPARIAN ZONES AT LARGE SCALE IN THE BRAZILIAN SAVANNAH

Dissertação apresentada ao Programa de Pós-graduação em Recursos Hídricos e Saneamento Ambiental da Universidade Federal do Rio Grande do Sul, como requisito parcial à obtenção do grau de mestre.

Orientador: Walter Collischonn

PORTO ALEGRE

2020

Fontana, Rafael Barbedo
IDENTIFYING AND ASSESSING VEGETATION BEHAVIOUR IN RIPARIAN ZONES AT LARGE SCALE IN THE BRAZILIAN SAVANNAH / Rafael Barbedo Fontana. -- 2020.
54 f.
Orientador: Walter Collischonn.

Dissertação (Mestrado) -- Universidade Federal do Rio Grande do Sul, Instituto de Pesquisas Hidráulicas, Programa de Pós-Graduação em Recursos Hídricos e Saneamento Ambiental, Porto Alegre, BR-RS, 2020.

1. Riparian zones. 2. Remote sensing. 3. Data analysis. I. Collischonn, Walter, orient. II. Título.

Rafael Barbedo Fontana

IDENTIFYING AND ASSESSING VEGETATION BEHAVIOUR IN RIPARIAN ZONES AT LARGE SCALE IN THE BRAZILIAN SAVANNAH

Dissertação apresentada ao Programa de Pós-graduação em Recursos Hídricos e Saneamento Ambiental da Universidade Federal do Rio Grande do Sul, como requisito parcial à obtenção do grau de mestre.

Aprovado em: Porto Alegre, 09 de março de 2020.

_____

Prof. Dr. Walter Collischonn – IPH/UFRGS
Orientador

_____

Prof. Dr. Anderson Luis Ruhoff – IPH/UFRGS
Examinador

_____

Prof. Dr. Alfonso Risso – IPH/UFRGS

Examinador

_____

Prof. Dr. Paulo Tarso Sanches de Oliveira – UFMS
Examinador

Agradecimentos

Ficam aqui, na única página deste documento escrita em língua portuguesa, os meus agradecimentos a todos que de alguma forma contribuíram para a realização desta dissertação e da minha evolução pessoal e profissional neste período:

- Ao professor Walter, pela orientação e por seus ensinamentos e entusiasmo em hidrologia. Aos professores e amigos Anderson, Fernando Fan e Rodrigo, por todo conhecimento transmitido e pela ótima convivência nesses anos. Aos demais professores membros da banca Alfonso Risso e Paulo Tarso, pelas excelentes contribuições e sugestões nessa pesquisa.
- Aos colegas e amigos do grupo de pesquisa HGE e do IPH como um todo, pela convivência do dia-a-dia, rodas de chimarrão, discussões e momentos descontraídos, em especial Fran, Ju, Aline, Ayan, Mel, JV, Rê, Camila, Joãozinho, Hugo, Clebinho, Siqueira, Sly, Léo, Matheus, Artur.
- Á CAPES pela bolsa de estudos e à UFRGS e ao IPH com toda sua estrutura e seus funcionários, sem os quais esse trabalho não poderia ter sido realizado.
- À minha família, meus pais Andiara e Jackson, minhas irmãs Ana Carolina e Antonia e à minha dinda Cláudia por toda estrutura e apoio emocional que me permitiram chegar até aqui.

Abstract

Riparian zones (RZs) have a clear distinct behaviour than the rest of the landscape. Particularly in water-limited regions, such as the Brazilian Savannah (Cerrado biome), where dry season may extend 5 months, the difference between riparian and upland zones is highly pronounced due to vegetation water access to groundwater, and this can have implications on the climatic and hydrological cycles. In order to quantify this difference at large-scale, it was herein proposed to (1) map RZs using topographical information, (2) investigate how land cover is distributed among topographic gradients and (3) investigate vegetation behaviour through remote sensing vegetation measurements and evapotranspiration (ET) estimation. A 140,000 km² upland region inside the Cerrado biome, called the Urucuia aquifer system, was chosen as study site. The region has seen a huge agricultural expansion during the last decades, with mechanized and irrigated crops increasingly using water from its underground reserves, which associated with climate change can have a big impact on the ecosystem, and understanding the role of RZs can be essential to quantify this impact. The height above nearest drainage (HAND) index was used to map RZs, by visually assessing bellow which values the index provided a reasonable RZ buffer comparing with Google Earth imagery. We also used HAND to quantify across its values the historical land cover distribution obtained by the MapBiomas database, and analyse vegetation behaviour in RZs and upland zones (UZs) using remote sensing vegetation measurements of normalized difference vegetation index (NDVI) and normalized difference moisture index (NDMI) and ET estimation from the surface energy balance algorithm for land (SEBAL). A necessary step for HAND computation is a defined stream network, for which the main challenge is identifying channel heads. Herein it was developed an algorithm that produced a varying draining area threshold (vDAT) map for channel initiation, using the topographic position index (TPI) as an auxiliary variable. This algorithm was tested using MERIT-DEM. With the stream network, HAND values bellow 5 m provided the best RZ buffer. As for land cover distribution, we captured that forests naturally occur more densely in the extreme values of HAND (very shallow and very deep) and that farmland historical occupation in the Urucuia region occur more in the upper portions of the terrain, possibly due to soil conditions stablished during landscape formation and evolution. As for vegetation activity, the land cover class seems to have more influence on vegetation behaviour than topographic position, for all indicators computed. Yet, NDMI values in Riparian Forests are greater than in Upland Forests, particularly towards drier conditions, in terms of both seasonality (drier months) and inter-annual variability (drier years). Despite this indication of more water available in RZs than UZs, the ET estimation could not capture these differences, possibly due to difficulties in estimating this variable in natural vegetation with high degree of water stress.

Key-words: Riparian Zones. Brazilian Savannah. Cerrado Biome. Remote Sensing. Vegetation Indices. Evapotranspiration estimation. Height Above Nearest Drainage.

Contents

1. Presentation

1.1. Introduction

Hydrological realistic physical representation, in terms of process and spatial complexity, is desirable in order to access the impacts of climate change, land use change and to allow better climatic and hydrological forecasts. However, hydrological behaviour at large scale is still poorly understood, mainly because of the lack of observable parameters at relevant catchment scale and process complexity representation. An alternative to landscape heterogeneity representation is grouping landscape elements in terms of their hydrological similarity.

A variable with great potential in this regard is topography, as it has a clear influence on catchment processes across different spatial scales and landscapes, such as flow rate and direction, groundwater level, recharge and discharge areas, soil storage, rooting depth, vegetation cover and geology. Using topography to link landscape by hydrological similarity is not new. Still, there is a lot to be explored in this type of application.

A particular case where this application can be useful is in assessing information in Riparian zones (RZs). as they play important roles in ecosystem functioning and water quality controls and there are reasons to believe that they play a more relevant role in large-scale water balance than their small area extent would suggest. Particularly in water-limited regions such as the Brazilian Cerrado, where dry seasons may extend up to 5 months, RZs provide a valuable source of water for ecosystem and social functioning.

RZs have been drawing attention recently, mainly because of human land use expansion and climate change. In the Cerrado biome, last decades have seen a huge spatial expansion of farmlands, mostly destined to pasture and croplands. Moreover, precipitation in the last years is below long-term average and climate change studies indicate an even drier climate in the future. All these factors drive attention to the need of proper management in these regions, in order to satisfy both socio-economic and ecosystem water demands.

A particular region inside the Cerrado, called the Urucuia Aquifer System, is of strategical importance in Brazilian water management, mainly because its groundwater is responsible for maintaining essential environmental services, such as providing water to sustain the baseflow of the São Francisco River during dry months. This region has seen a massive agricultural expansion in recent years, specially irrigated, with increasing water use, and its effects on environmental resources have yet to be fully understood. Associated with climate change, this can have a profound impact on the surrounding environment. Understanding the role of RZs in this system can be essential in quantifying this impacts, as they are believed to play a huge role in environmental controls

First, however, we must know how to assess information on these ecosystems' location and water demands. Assessing information on RZs at large scale, however, is not a simple task. Remote sensing may provide valuable information. Measurements and estimations provided by remote sensing that have a clear influence on RZs are related to topography, vegetation activity, evapotranspiration, soil moisture and water storage.

1.2. Objectives

The main objective of this study is to investigate how RZs' vegetation behaviour differs from other terrain portions in regions with consistent dry season, such as the Brazilian Neo-Tropical Savanna (Cerrado), at large scale, using widespread remote sensing information. In order to quantify this difference, it is herein proposed to (1) map RZs using topographical information, (2) investigate how land cover is distributed among topographic gradients and (3) investigate vegetation behaviour through remote sensing vegetation measurements and evapotranspiration (ET) estimation. The Urucuia Aquifer System (140,000 km²) was chosen as study site for its environmental and management importance among the Brazilian territory.

2. Hydrological processes in riparian zones

Water falls on land surface in form of precipitation. The water that does not fall directly on water bodies passes through processes of interception, infiltration, evaporation, transpiration and lateral movement before reaching water bodies or returning back to the atmosphere. These processes are influenced by several characteristics of the landscape, such as vegetation cover, soil type and geology. An important factor that controls those landscape characteristics and also water movement directly is topography.

As water movement is largely controlled by gravity, topographic gradients have huge importance in determining water fluxes in terms of velocity and accumulation. These fluxes can be more easily understood from a hillslope perspective. In this perspective, landscape may be divided into four components: drainage, riparian zone, hillslope and plateau. Identifying these components on the landscape is not easily done; however, the profile scheme presented in Figure 1 is helpful for understanding some processes.

The riparian zone (RZ) can be defined as the interface between aquatic and terrestrial domains. The upland zone (UZ) is divided into hillslopes and plateaus, where their separation lies on topographic gradients, which are greater in hillslopes. Usually, hillslopes are in transition between plateaus and riparian zones and plateaus are in transition between two hillslope systems. This is not always the case, as landscape presents complex geomorphologic features and component definition is not so clear. However, the scheme of Figure 1 is a well-suited general case for understanding.

Precipitation and soil interactions generates fluxes of overland flow and infiltration. The latter is the process of water entering the soil from ground surface. Water that infiltrates is stored in the soil or moves further by processes of throughflow or percolation. Throughflow is the fast-horizontal water movement in soil upper layers. Percolation happens at the interface between the upper and deeper layers, where water moves to the saturated region of the soil, called water table, aquifer or groundwater. Water supply to the aquifer through percolation is the process called groundwater recharge. Groundwater movement is very slow. The water table usually follows topographic gradients (Hubbert, 1940) until water flows to water bodies – rivers, lakes, pounds, or sea. This process is called groundwater discharge. It is responsible for maintaining water on rivers and lakes during dry periods.

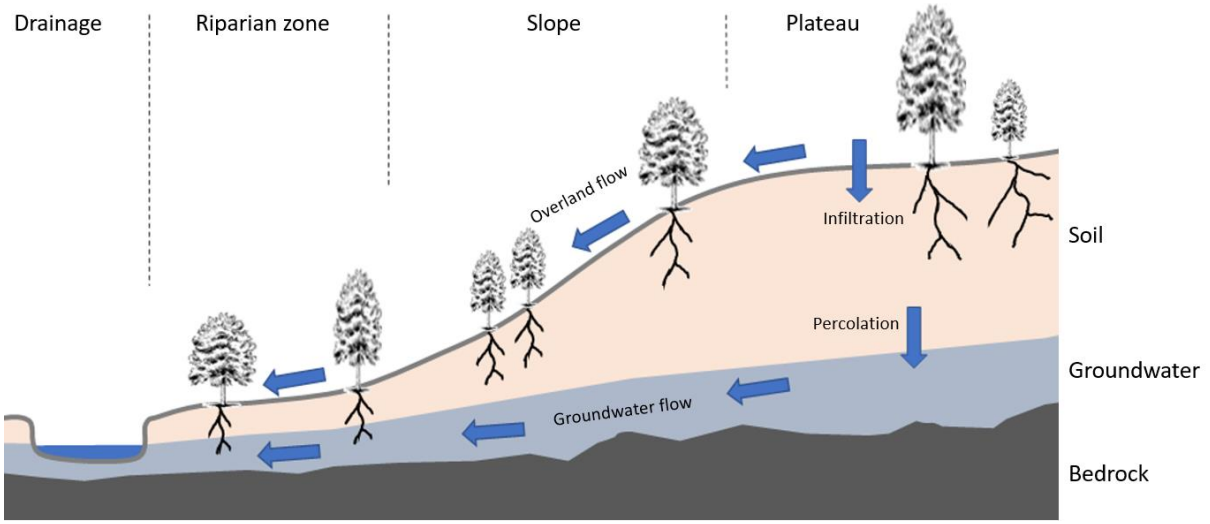

Figure 1: Hillslope perspective showing main landscape elements.

The water stored in the soil provides moisture to plants. In the root zone, vegetation collects water from soil and returns it back to the atmosphere through transpiration. The vegetation characteristics in a region are dictated, mainly, by soil water availability. It can be permanently wet, with cycles of flooding, or adapted to periods without water varying from a few days to several months. Riparian zones, however, generally have a pronounced difference than the rest of the landscape. In water-limited regions, where vegetation is adapted to long dry periods, the riparian system usually falls in the permanently wet category, provided by groundwater; whereas in wet regions, where vegetation is constantly wet, riparian vegetation is controlled by flood pulses and erosion and deposition processes (Hupp and Osterkamp, 1996). Figure 2 shows a comparison between two undisturbed areas with and without water limitation.

The preservation of wetlands and riparian zones world-wide have been drawing attention recently, because of their economic and ecological value and sensitivity to water level changes (Baker et al., 2006; Scott et al., 2014; Stromberg et al., 1996; Tabacchi et al., 2000). The hydrological processes in these areas are of great relevance, as they can have important roles in amplifying catchment response to climatic variability, by increasing evapotranspiration in drier periods (Lupon et al., 2018; Scott et al., 2008, 2014; Serrat-Capdevila et al., 2011; Tabacchi et al., 2000).

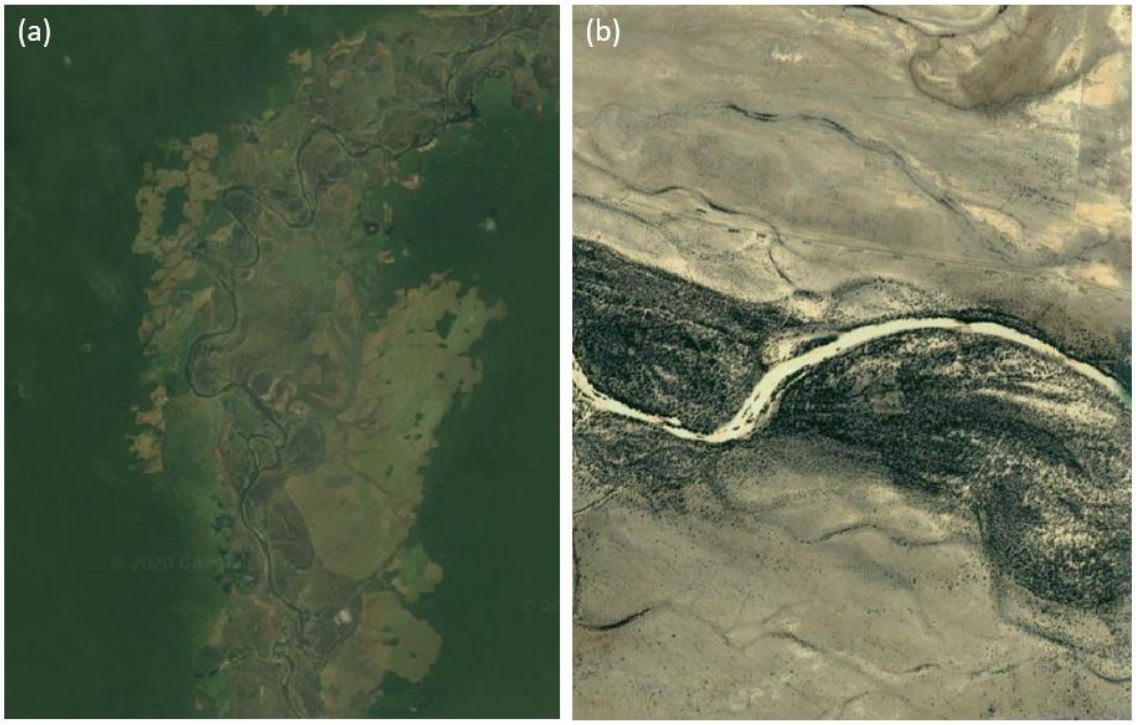

Figure 2: Riparian zone distinct vegetation cover compared to upland zone in (a) wet region – tropical Congo forest – and in (b) semi-arid region – Australia. Source: Google Earth.

3. Tools for RZ identification

3.1. Hydrological similarity

Landscape factors, such as climate, topography, vegetation and soil have influence on each other's long-term formation. This concept is called landscape coevolution or catchment coevolution (Sivapalan and Blöschl, 2015; Troch et al., 2013, 2015). We can imagine the long-term physical processes of erosion and sediment deposition that are shaped by topographic gradients (slopes) and chemical processes of weathering that are shaped by water content (Lepsch, 2016). As a self-organizing system, therefore, landscape features are developed in a way to efficiently fulfil hydrological processes of drainage and water storage (Savenije, 2010). The partitioning and destination of incoming and outgoing water fluxes are mostly defined by soil moisture conditions, and its spatial distribution plays important roles in controlling infiltration, evapotranspiration, recharge and runoff generation (Beven and Kirkby, 1979; Dunne and Black, 1970; Famiglietti et al., 1998; Moore et al., 1991; Nobre et al., 2011; Sørensen et al., 2006).

Considering that many points in a region have similar soil moisture characteristics – and, by consequence, similar hydrological behaviour – they can be grouped in terms of hydrological similarity (Beven, 2012; Flügel, 1997). Separating the landscape in units of hydrological similarity, therefore, is a very useful tool in hydrology for understanding governing processes on soil and vegetation. It allows hydrologists to simplify landscape physical representation by accounting processes in a lumped way, while information can be accessed in a distributed way. Hydrological modelling has been using this conceptual approach for decades for distributed applications (Arnold et al., 1993; Beven and Kirkby, 1979; Collischonn et al., 2007; Savenije, 2010) as a less demanding alternative to the complex and high computational cost physically-based approaches (Abbott et al., 1986; Kollet and Maxwell, 2006).

Topography can be a valuable tool in grouping landscape features, as it greatly influences local energy and water budget, and so hydrological conditions such as groundwater flux and soil moisture are strongly controlled by it. Hydrological conditions of fluxes and accumulation controlled by topography, hence, can also be used as proxy for soil formation (Behrens et al., 2010; Kopecký and Čížková, 2010; Lin and Zhou, 2008; Park and van de Giesen, 2004; Pelletier and

Rasmussen, 2009) and vegetation cover (Bartels et al., 2018; Fan, 2015; Fan et al., 2017; Furley, 1999; Kopecký and Čížková, 2010).

3.2. Topographic indices for RZ identification

Topography information is widely available today through digital elevation models (DEM), and is of great importance in recent application of hydrological sciences. Topographical indices to identify wet areas are being used for a long time, and continue to evolve in all kinds of hydrology-related studies. A notable example is the topographic wetness index (TWI), developed by Beven and Kirkby (1979) to run within the TOPMODEL. It is defined by:

$$ln(a/\tan b),$$

where a is the local upslope area draining to a certain point per unit contour length and $\tan b$ is the local slope gradient. The index is a measure of the predisposition of the soil in a specific point within a catchment to become saturated. It has been widely applied in hydrologic research and modelling. Until the early 2000's, most research regarding topographic controls on hydrologic conditions focused on improvements in obtaining the TWI (Tarboton, 1997), as it was early recognized its high sensitivity to scale of the DEM used (Ågren et al., 2014; Blöschl and Sivapalan, 1995) and to the algorithm used to compute flow directions (Kopecký and Čížková, 2010). The matter with the physics of the TWI, although, is that it only considers upslope and local topography, neglecting downslope controls in soil moisture conditions, demonstrated in several studies to be strong (*e.g.* Crave and Gascuel-Odoux, 1997; Hjerdt et al., 2004).

To overcome these issues, some other topographic indices have been proposed, considering each cell value as a function of a downslope cell following the flow direction path, either by distance, difference in elevation or both. The downslope cell is chosen by some criterion, which may be the catchment outlet cell (Crave and Gascuel-Odoux, 1997), a cell where head difference equals some threshold (Hjerdt et al., 2004) or a cell in which a channel exists (Murphy et al., 2009; Nobre et al., 2011).

It has been demonstrated that these approaches have advantages over the classic TWI on predicting soil-water proprieties (Ågren et al., 2014; Gharari et al., 2011; Murphy et al., 2009, 2011; Oltean et al., 2016). In considering each cell as a function of the closest channel following the flow path,

we can highlight two indices that were developed at about the same time and provide the exact same result: the depth to water (DTW) (Murphy et al., 2009, 2011) and the height above nearest drainage (HAND) (Nobre et al., 2011; Rennó et al., 2008).

3.2.1. The Height Above Nearest Drainage (HAND)

The HAND algorithm (Nobre et al., 2011; Rennó et al., 2008) gives the vertical distance of a given grid point to the nearest drainage following the flow direction path. Grid points are, then, hydrologically connected accordingly to their respective draining gravitational potential. The basic assumption of the index is a classical idea that topography follows water table (Hubbert, 1940). As water content have been observed to have major controls on landscape (Christoffersen et al., 2014; Detty and McGuire, 2010; Fan, 2015; Le Maitre et al., 1999; Miguez-Macho and Fan, 2012), cells with the same gravitational potential would have similar hydrological behaviour that match with runoff generation mechanisms, soil proprieties and land cover characteristics (*e.g.* Gao et al., 2018; Gharari et al., 2011; Savenije, 2010; Schietti et al., 2014).

The resulting HAND map (Figure 3) could be interpreted as a normalized altitude map in which low values correspond to wet areas (riparian zone), and higher values would correspond to hillslopes and plateaus, depending on other topographic features, such as local slope (Savenije, 2010). Riparian zone buffering is one of the most potential applications of HAND (Kuglerová et al., 2014; Murphy et al., 2011; White et al., 2012), as giving a drainage potential to a point based on drainage location can be very useful for identifying similar hydrological landscape elements.

HAND computation requires a hydrologically coherent DEM (with resolved sinks), computed single flow directions (as multiple flow directions would result in more than one value for each cell) and a defined drainage network. It has the advantage of being little dependent on DEM resolution and on the flow direction algorithm used (Ågren et al., 2014; Hjerdt et al., 2004), although its performance is very sensitive to a well suited drainage definition. All HAND applications reviewed herein used very simple methods for drainage extraction. Most recent hydrological research has not given much attention on this matter, although channel definition had considerable effort in the 1980s. Next section will discuss drainage extraction in DEMs with more detail.

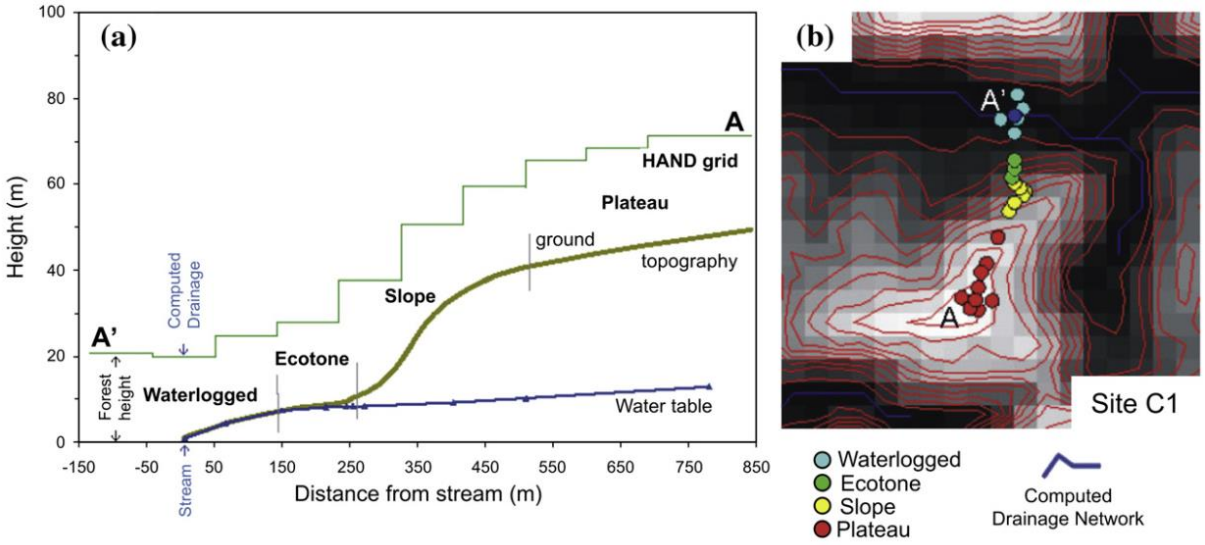

Figure 3: HAND application in the Amazon, (a) cross-section with hydrological hillslope (A-A') relating vegetation cover and water table level and (b) ground-truth points onto SRTM-based HAND grid. Source: Rennó et al. (2008).

3.3. Drainage extraction from Digital Elevation Models (DEMs)

Points at which runoff is sufficiently concentrated that fluvial processes dominate over slope processes represent a drainage channel (O'Callaghan and Mark, 1984). The definition of a drainage channel in a DEM grid is a necessary step in several hydrological applications such as the HAND. The usual GIS approach to define drainage network is by setting a draining area threshold (DAT), *i.e.* a pixel value representing channel heads on a flow accumulation grid map, above which every pixel is considered part of the drainage network. So, by testing different DATs and observing satellite images or existing drainage maps one can see what DAT fits best to the actual drainage channel. Most applications in catchment hydrology use a single value for DAT, but this may lead to considerable errors, because draining area is not the only topographic feature controlling channel initiation.

Steeper areas usually require less draining area than flatter ones. Channel heads have been reportedly associated with the convexo-concave terrain profile, *i.e.* break of slope, which is a result from erosion processes of flow transition from diffusive to concentrate (Howard, 1994; Montgomery and Dietrich, 1988, 1989). Channel initiation contributing area are shown to vary as a function of local topographic slopes (Montgomery and Dietrich, 1988, 1989). However, local slopes are highly dependent on DEM resolution because they only consider adjacent cells for

computation, therefore using an area-slope relationship is only suitable when applied to fine scale DEMs, which are not widely available and often very hard to obtain. To date, all applications of drainage extractions using slope-area relationships relied on fine-scale DEMs (*e.g.* Menduni et al., 2002; Passalacqua et al., 2010; Pelletier and Rasmussen, 2009; Tarboton and Ames, 2001).

For large-scale applications and to overcome the scale issue, the topographic position index (TPI) index can be used to assist stream network definition. First introduced by works of Guisan et al. (1999) and Weiss (2001), it was proposed to compute different landforms. TPI is calculated as the difference between the original DEM pixel value and the average value of its neighborhood defined by a selected radius. In practice, it is the difference from mean elevation (Wilson and Gallant, 2000), where the mean elevation grid is equivalent to a low-pass filter using a circular window (Burrough et al., 1998). Negative values indicate points lower than its average surroundings (valleys), while positive values indicate a position higher than the average (ridges), and values close to zero are slopes or flat areas. The radius will determine the scale of the landscape feature: while large radius values correspond to major landscape units, small values will reveal smaller features (Figure 4).

In its suggested application, two different radii are selected – 300m and 2000m, to represent small and large neighbourhoods – and different slope position classes are attributed to each pixel based on breakpoints (thresholds) of the combined TPI grids. Weiss (2001) recommends values of radii and breakpoints to be adjusted for each particular landscape or problem to be solved, as well as incorporation of additional metrics, such elevation variance or local slope. The TPI has shown promising applications in landform classification (De Reu et al., 2013; Riley et al., 2017; Tagil and Jenness, 2008) and wetland analysis (Mokarram et al., 2015). In the porpoise of this study, radii and breakpoints can be used to define DATs, and be useful for drainage extraction. This application has never been used before and it is one of the innovative aspects shown herein. Further explanations of this application will be given in the Methods section.

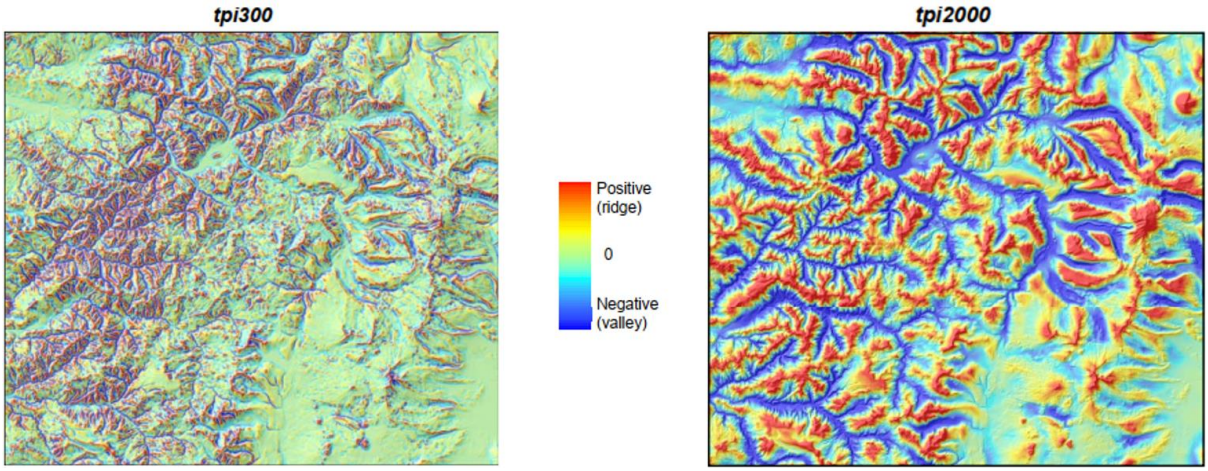

Figure 4: Representation of TPI maps computed at two different radius scales – 300m and 2000m. Source: Weiss (2001).

4. Monitoring vegetation activity through remote sensing

The acquisition of information of some propriety of and object or phenomenon recorded without physical contact with the object or phenomenon can be called remote sensing. The recording device can be anywhere ranging from just above the surface of the Earth to hundreds of kilometres away in space. It is based on electromagnetic wave interactions between the signal emitted by the device with Earth's land surface, ocean and/or atmosphere. The variable wanted is not the actual measured response by itself, but is inferred by the principles of electromagnetic radiation physics coupled with ground data (Jensen, 2006).

4.1. Spectral indices

The spectral signature of plants is strongly linked by its chlorophyll and water contents and its leaf structure (Figure 5). Chlorophyll is responsible for a markedly absorption in the regions of blue and red bands. Three absorption bands in the middle infrared (MIR) region (water absorption bands) determine how hydrated the leaf tissue is. At near-infrared (NIR) wavelengths, there is a strong reflectance caused by scattering in the spongy mesophyll, the deeper layers of the leaf (Purkis and Klemas, 2011).

From the use of red and infrared bands, it is possible to obtain vegetation indices - dimensionless, radiometric measures that indicate relative abundance and activity of vegetation, like leaf-area-index (LAI), percentage green cover, green biomass, absorbed photosynthetically active radiation (APAR) and chlorophyll content (Jensen, 2006). Some of them can be visualized in *Table 1*, where ρ is the reflectance of the band (*Red, NIR, MIR*), G is a gain factor, L is canopy background adjustment factor, C_1 and C_2 are coefficients for atmospheric aerosol correction.

NDVI provides information about vegetation photosynthetic activity or LAI and is used to monitor vegetation activity and growth. NDMI gives vegetation water content and has more closely relationship to plant biomass and water stress than NDVI. SAVI improves vegetation activity information with adjustments to minimize soil "noise" in the NDVI. EVI is used as well to correct soil noise in NDVI, and it also increases sensitivity on high plant biomass, useful in densely forested areas.

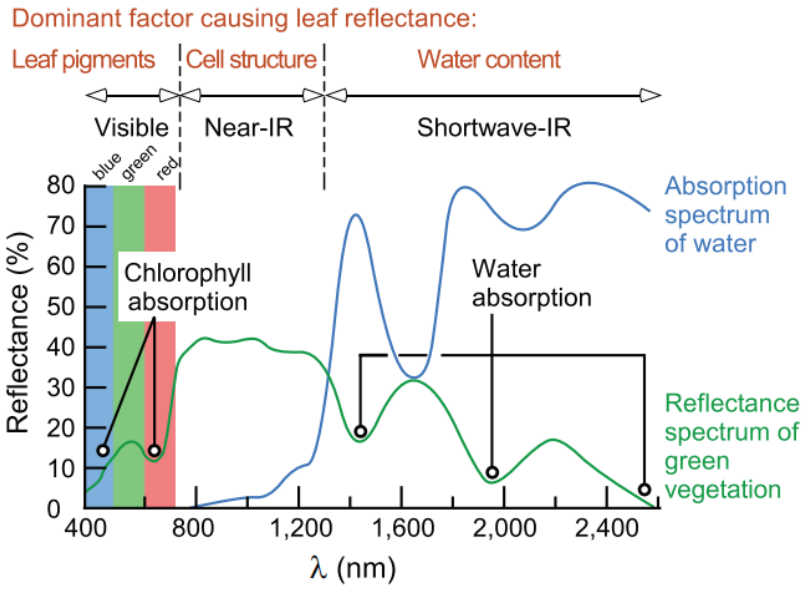

Figure 5: Vegetation and water spectral signature. Source: Purkis and Klemas (2011).

Normalized Difference Vegetation Index (NDVI)	$NDVI = \frac{\rho_{NIR} - \rho_{Red}}{\rho_{NIR} + \rho_{Red}}$
Normalized Difference Moisture Index (NDMI)	$NDMI = \frac{\rho_{NIR} - \rho_{MIR}}{\rho_{NIR} + \rho_{MIR}}$
Soil Adjusted Vegetation Index (SAVI)	$SAVI = \frac{(1+L)(\rho_{NIR} - \rho_{Red})}{\rho_{NIR} + \rho_{Red} + L}$
Enhanced Vegetation Index (EVI)	$EVI = G \frac{\rho_{NIR} - \rho_{Red}}{\rho_{NIR} + C_1\rho_{Red} + C_2\rho_{Red} + L}$

Table 1: Remote sensing vegetation related indices. Source: Jensen (2006).

4.2. Evapotranspiration estimation

Another important information of vegetation signature is evapotranspiration (ET). There are several ways to estimate this variable through remote sensing data. Most common approaches rely on (i) physically-based equations such as the Penman-Monteith equation (Mu et al., 2007, 2011) or on (ii) surface energy balance methods (Allen et al., 2011; Bastiaanssen et al., 1998a; Liou and Kar, 2014). Physically-based ET estimations use vegetation indices and parameters associated with meteorological data to fill the equation variables. Energy balance approaches use surface

temperature, surface reflectance and NDVI, as well as their interrelationships to compute energy fluxes.

The advantage of energy balance based over vegetation-based methods is that actual ET rather than potential ET is computed – capturing ET reductions caused by stress of disease, salinity or shortage soil moisture. In these approaches, evapotranspiration is the residue of the energy balance equation:

$$LE = R_n - G - H \,, \tag{1}$$

where LE is latent heat flux, R_n is net radiation flux, G is soil heat flux and H is sensible heat flux. The net radiation flux at the surface R_n is obtained by subtracting all outgoing radiant fluxes from all income radiant fluxes, as

$$R_n = (1-\alpha)Rs_{down} + Rl_{down} - Rs_{up} - (1-\epsilon)Rl_{up}\,, \tag{2}$$

where Rs_{down} is incoming shortwave radiation, Rl_{down} is incoming longwave radiation, Rs_{up} is outgoing shortwave radiation, Rl_{up} is outgoing longwave radiation, α is surface albedo and ϵ is surface emissivity. Soil heat flux is computed by

$$G = \frac{R_n(T_s - 273.15)}{\alpha}(0.0038\alpha + 0.007\alpha^2)(1 - 0.98NDVI^4)\,, \tag{3}$$

where T_s is surface temperature (K). Sensible heat flux is

$$H = \frac{\rho\, c_p\, dT}{r_{ah}}\,, \tag{4}$$

where ρ is air density, c_p is specific heat of air (1004 J/kg/K), dT is temperature difference between two near-surface heights and r_{ah} is aerodynamic resistance (s/m). The parameter dT is obtained by assuming that it has a linear relationship with surface temperature T_s, and that in a cold pixel of the image LE is maximum and H is zero and in a hot pixel H is maximum and LE is zero. The aerodynamic resistance r_{ah} need to be calibrated by an iterative method described by Allen et al. (2013).

5. The Brazilian Neo-Tropical Savanna (Cerrado)

The central plateau region of Brazil is home to the Cerrado biome. It covers about 22 % of the Brazilian territory (an area of 2 million km²), being the second largest tropical ecosystem in South America. Because of its geographical location (uplands of Brazil), the biome is located at the headwaters of several South America's major rivers, including the São Francisco, Tocantins, Parnaíba, Paraná and Paraguay. Therefore, hydrological processes within the Cerrado biome play a substantial role on how those rivers behave under climate variability and change and other environmental stresses.

Figure 6: The cerrado region (red line) in the context of the major basins in the Brazilian territory.

Climate in Cerrado is majorly tropical, characterized by warm temperatures – averages from 20 to 26 ºC – and intermediate rainfalls – yearly averages varying from 750 mm (in the transitions with the semi-arid 'Caatinga' and 'Chaco') to 2000 mm (in the transitions with the humid 'amazon forest' and 'mata atlântica'), with a well-defined dry season, that happens from May to September and on winter months (June, July and August) rain is often absent (Eiten, 1972; Oliveira-Filho et al., 1989; Villalobos-Vega et al., 2014). The soils are mostly well-drained, dystrophic, acid and have high aluminium content (Ratter et al., 1997).

The region presents very rich savanna-like vegetation formations, comprising a great variety of forests and grasslands. Their physiognomic forms are usually classified into (a) 'cerradão', dense forests with closed canopy; (b) 'cerrado strictu-senso', woodlands and shrublands relative dense; (c) 'campo cerrado', low tree and shrub savannas; (d) 'campo sujo', grasslands with scattered shrubs; and (e) 'campo limpo', grassland savannas (Cole, 1960; Eiten, 1972). These are the main types of vegetation forms, which cover the most part of the Cerrado region across the interfluves.

Topographic position and gradient, which are indicators of groundwater level and drainage controls, have a clear influence on the occurrence of undisturbed Cerrado vegetation (Furley, 1999; Leite et al., 2018; Oliveira et al., 2017; Rossatto et al., 2012, 2014; Villalobos-Vega et al., 2014). Deep water tables, which occur at higher terrain elevations, are associated with dense woodland structures and more species diversity. Whereas in lowlands and valley floors, where water table is shallower and have greater fluctuation regimes, there is a predominance of grassland physiognomies. This can be attributed to the intolerance of cerrado trees to waterlogging and flood pulses (Eiten, 1972; Oliveira-Filho et al., 1989; Ratter et al., 1997).

However, in small portions along the valley floors, close to streams, evergreen gallery forests also occur, composed mostly by palm trees, called 'veredas'. These gallery forests are adapted to a constant wet environment, promoted by poorly drained hydromorphic soils in shallow water table zones along intermittent rivers (Eiten, 1972; Furley, 1999; Maillard et al., 2008). These conditions are sustained by groundwater throughout the commonly long dry periods in the Cerrado, making this riparian vegetation highly groundwater dependent.

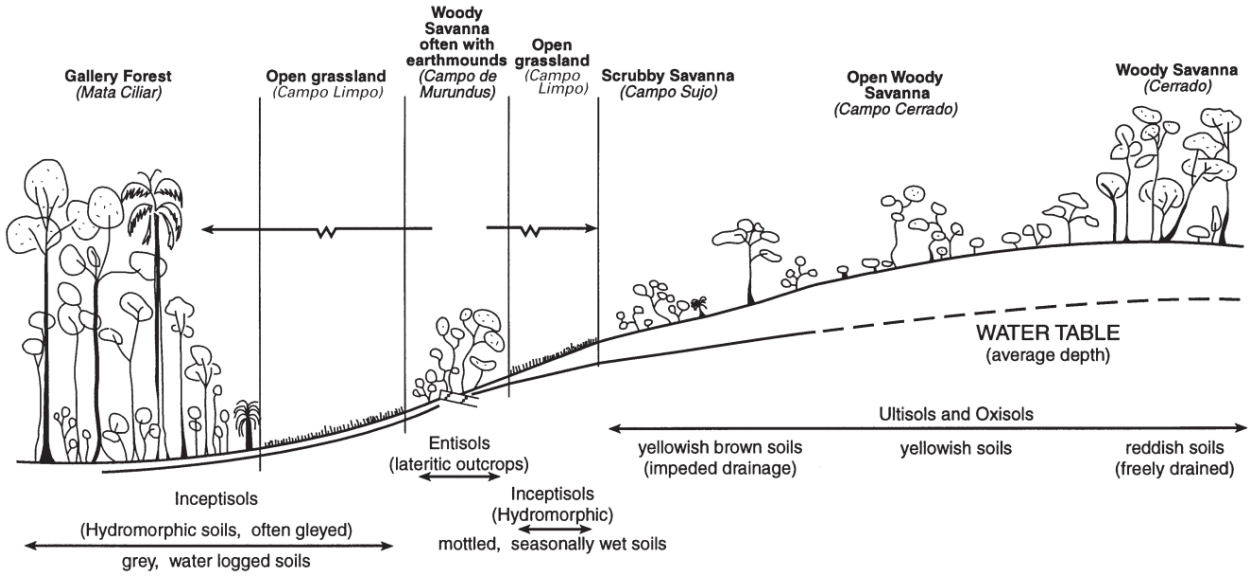

Figure 7: The influence of topography and drainage in vegetation and soil forms of the Cerrado. Source: Furley (1999).

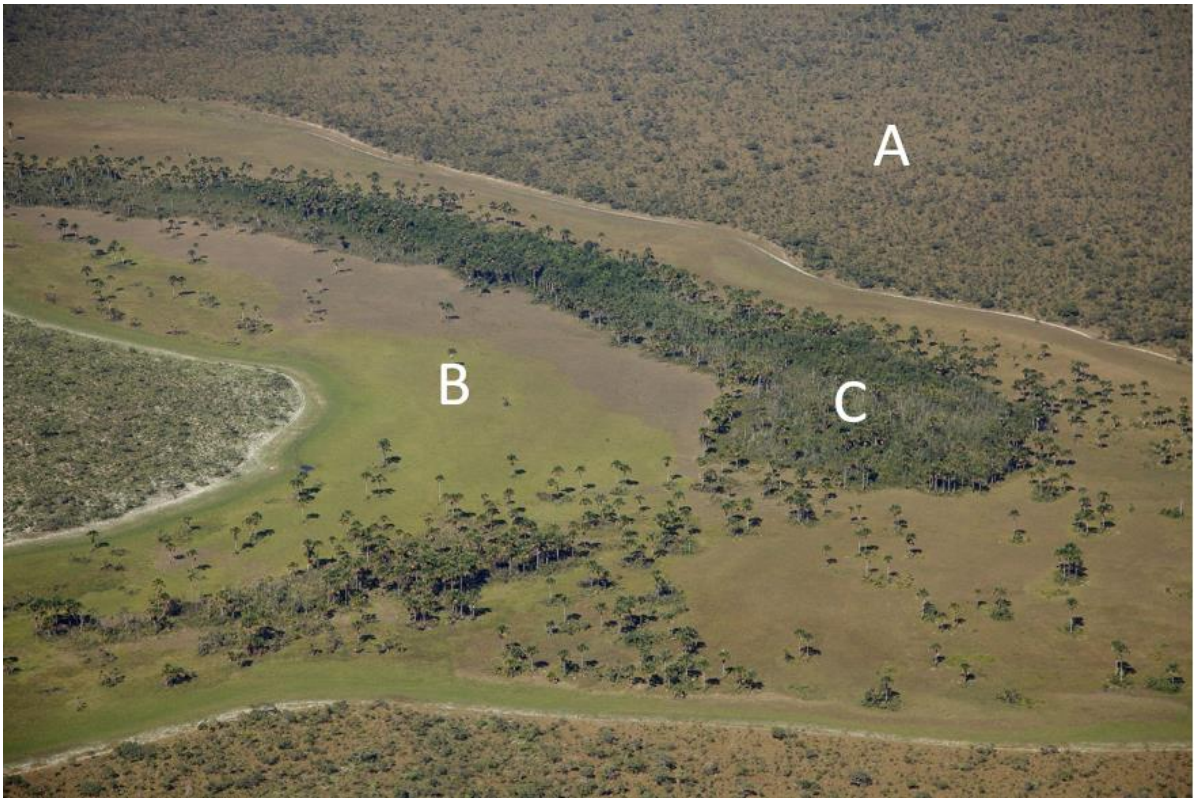

Figure 8: Cerrado vegetation along a valley floor. (A) Open woody savannah, 'campo cerrado'; (B) Open grassland, 'campo limpo'; (C) Gallery forest, 'vereda'.

6. Methods

The goal of this study was to use tools to identify and assess information in riparian zones at large-scale. In water-limited regions, RZs have a clear distinct vegetation, related to root zone access to water table in the dry season. The HAND index may be a good metric for RZ identification, as seen in section 3.2.1, because water table follows topography at large scales and RZs are close to streamlines. Therefore, by identifying streamlines and using a HAND value threshold to buffer RZs using satellite imagery observation, we could then assess information in these zones.

The main problem with drainage network extraction is that it is very hard to obtain by traditional GIS methods or existing databases. We wanted to provide a general tool for large scale streamline delineation, allowing to treat all sorts of cases encountered in heterogeneous landscapes and climate domains. By testing different GIS approaches for obtaining drainage location, we developed an algorithm to define drainage initiation and, consequently, have a reasonable map of drainage locations. With this map we could compute HAND and buffer the RZs.

Next step would be assessing landscape information and verify signature differences between RZs and UZs, analysing (1) land cover distribution, (2) vegetation spectral indices and (3) ET estimation over HAND gradients. For application site of this process, it was chosen a region inside the Cerrado biome, in Brazil, called the Urucuia Aquifer, which will be presented next.

6.1. Study site: The Urucuia Aquifer System

The Urucuia Aquifer System is situated among the Brazilian states of Bahia, Minas Gerais, Goiás, Tocantins, Maranhão and Paraíba; and is entirely covered by the Cerrado biome, covering an area of about 140,000 km². It is an upland aquifer system, in which headwaters provide large Brazilian basins, such as the São Francisco, the Tocantins and the Parnaíba.

Climate in the region is tropical sub-humid, with average daily temperatures ranging from 18ºC in winter to 28ºC in summer. Average annual rainfall is about 1400mm in the northwest portion and decreases to about 1000mm in the southeast, with standard deviations between 200 and 300 mm. The dry season extends from May to September, when rainfall is nearly absent. Reference

evapotranspiration is minimum at the end of the wet season (3.8mm/day) and maximum at the end of the dry season (6mm/day).

The whole region has a strong presence of flat-topped mountain ranges, very common in the Brazilian Highlands, called “chapadas”, naturally dominated by dense woodlands and where agriculture expansion has been greater in recent years. These formations are intersected by large valley floors, where vegetation is mostly composed of grasslands and open-wooded savannahs. Within these valley floors, following intermittent rivers, the landscape gives place to evergreen gallery forests called “veredas”.

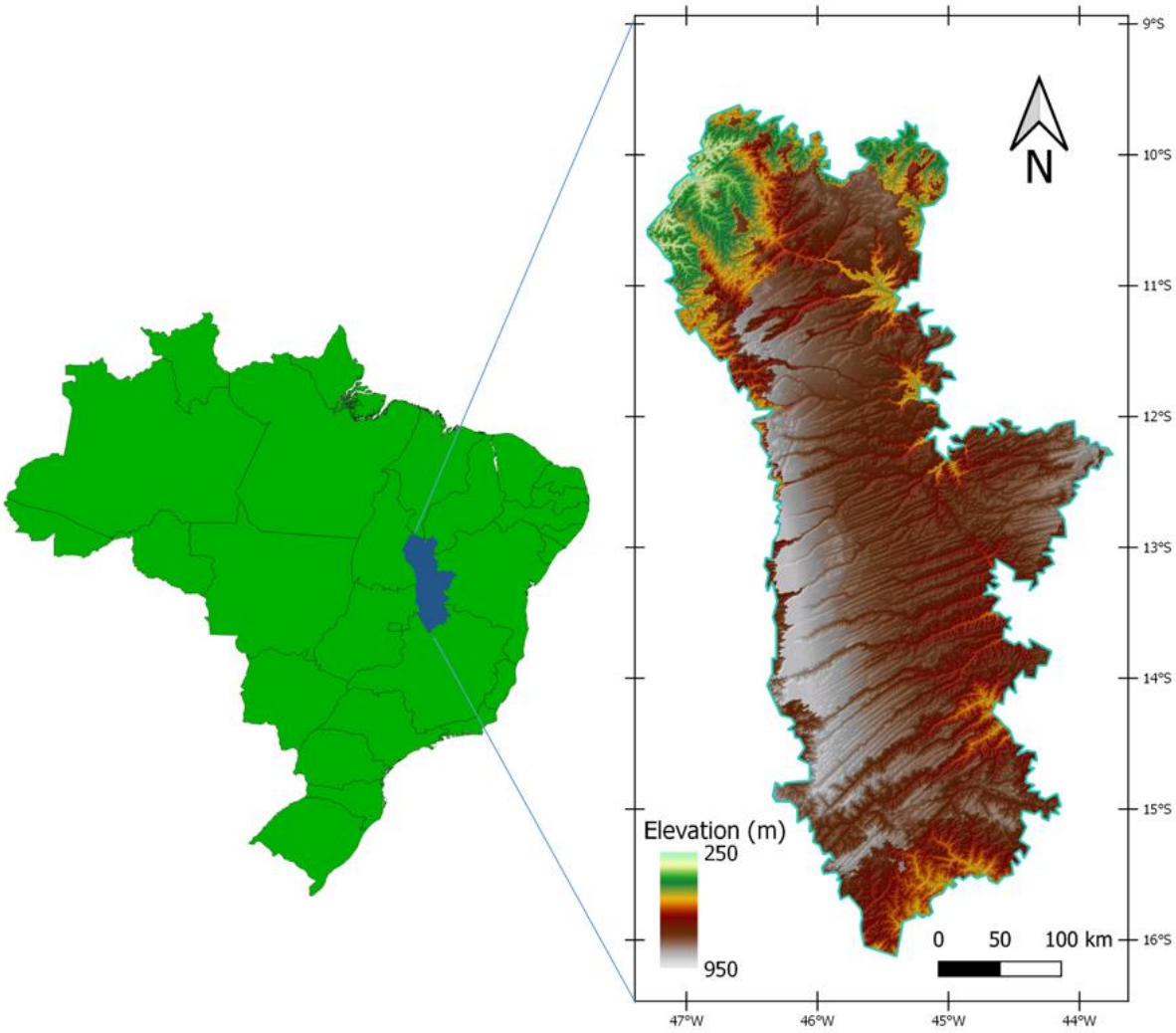

Figure 9: The Urucuia Aquifer in the context of the Brazilian territory

For the last decades, the Urucuia region has been one of the main spots of agricultural expansion in Brazil, mostly by mechanized and irrigated crops, with increasing water use (Amorim Junior and Lima, 2007). The aquifer water availability, as well as the flow of water courses may be compromised by the cropland water use. There are already been reported reductions in wetlands, floodplains and river flows, with some stretches even drying out (Amorim Junior and Lima, 2007; Gonçalves et al., 2018).

6.2. Drainage extraction – varying draining area threshold (vDAT) for channel initiation

A series of topographic criteria were used to make a varying draining area threshold (vDAT) map. Traditionally, a single value of DAT is used alongside with flow directions and flow accumulation maps to set drainage locations. We observed that DAT was minimum at steeper areas (about 5km²) and maximum at plain areas (about 500km²). The vDAT map, then, is a binary map with these two thresholds. Pixels in which the topographic criteria identified as channel heads, DAT values were 5km², and other pixels DAT values were 500km². A flowchart with the algorithm, is presented in Figure 10.

For the topographic criteria to identify channel heads, we used slopes and different radii of the topographic position index (TPI). Figure 11 presents examples of DEM and derived maps of the inputs used. First, we selected a slope threshold as a parameter, in which slopes above 5% were considered too steep to begin channels. After that, we selected two neighbourhoods – 300m and 9000m, which we are going to call tpi300 and tpi9000 – in combination with value thresholds in which a channel could probably begin, through a trial and error process. Pixel values with tpi9000 < -1.0m or tpi300 < -1.4m we considered as channel heads, as well as the combination tpi9000 < -0.2m and tpi300 < -0.6m.

After that, a filter to remove outlier pixel values was applied. For each pixel with DAT = 5km², if it not encounters other pixel with the same value in 3km following the flow direction, it was attributed a DAT value of 500km². This step was necessary because TPI maps with small neighbouring sizes present a large number of noisy values, and these values can have a great negative effect on the final drainage map.

With a drainage map defined, the computation of HAND is possible. Once a HAND map is computed, next step was defining a threshold HAND value to buffer riparian zones (RZ). We did this by visual assessment, comparing bellow which HAND values RZs would be better represented.

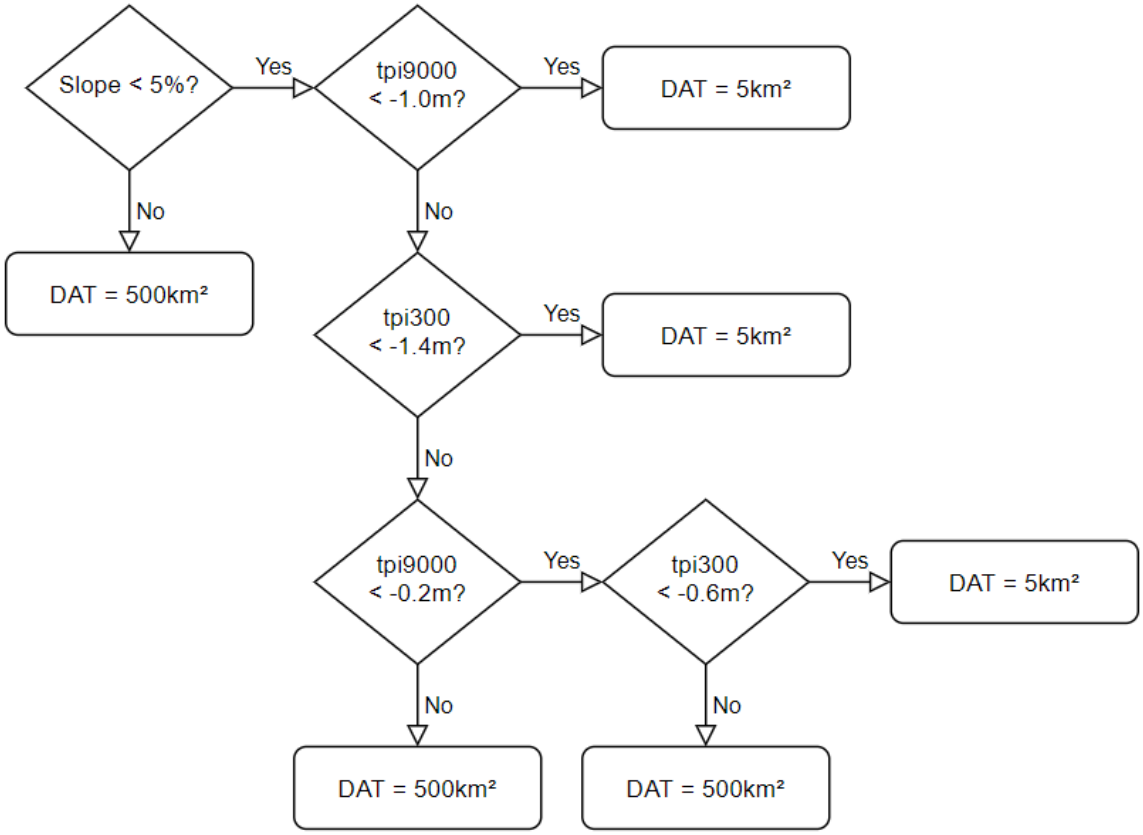

Figure 10: Flow chart of DAT map algorithm.

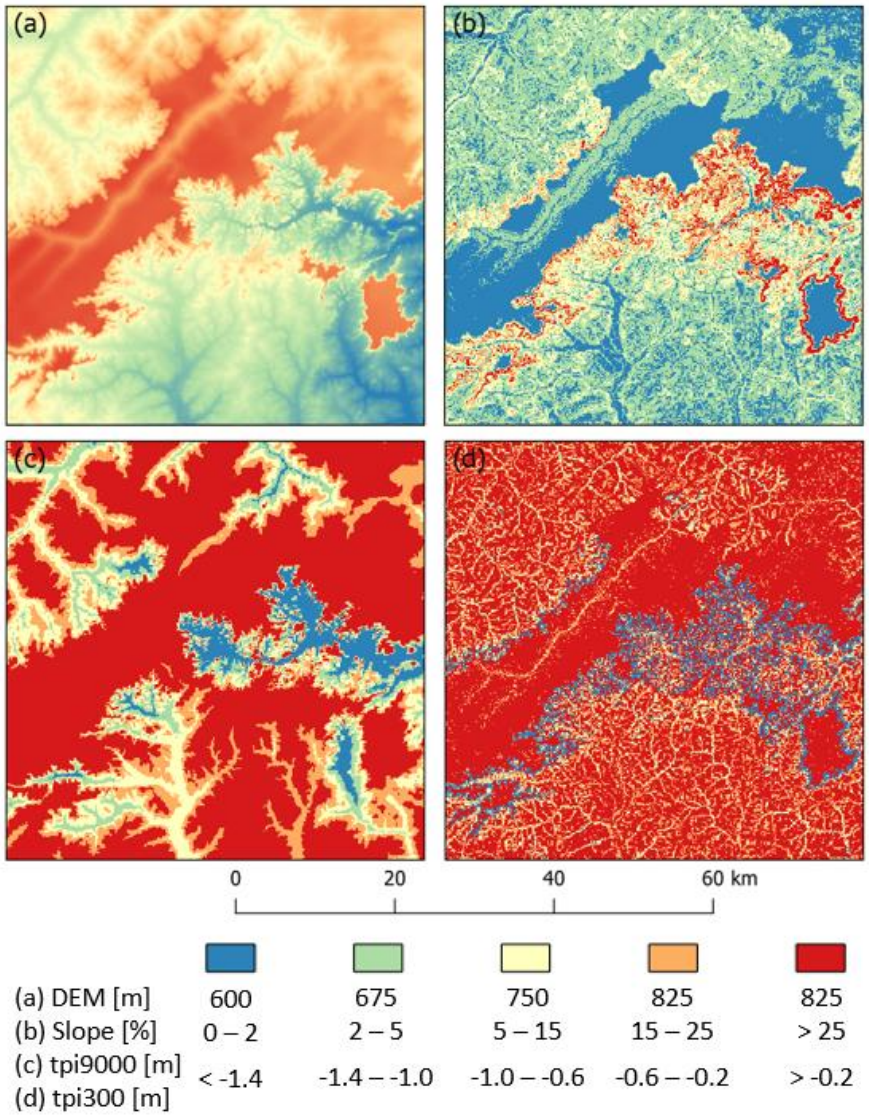

Figure 11: Examples of DEM itself and derived maps used as input for DAT map definition.

6.3. Datasets

6.3.1. DEM, flow directions and accumulated areas

For this study we used the Multi-Error-Removed Improved Digital Elevation Model (MERIT-DEM), which was elaborated by correcting major error components from existing DEM datasets, such as the SRTM, JAXA and AW3D (Yamazaki et al., 2017) . Flow directions and accumulated areas were taken from the MERIT Hydro database (Yamazaki et al., 2019), which is a suite of

global hydrography products produced on the MERIT-DEM. The whole dataset is at 3 arc-sec resolution (90 m at the equator).

6.3.2. Land cover

Land cover data were collected from the MapBiomas project database, which gives annual land cover maps from 1985 to 2018 for the whole Brazilian territory. The project is a collaborative network made by cloud machine learning processing and automated classifiers through the Google Earth Engine platform (Gorelick et al., 2017). The maps are produced through pixel by pixel classification of Landsat satellite imagery. More details in: http://mapbiomas.org.

The MapBiomas classification is divided into 33 classes. As our region is predominantly occupied (>99%) by forests, savannas, grasslands and farmlands, we neglected other land cover features. We used – for presentation simplification – 4 representative years (1988, 1997, 2006 and 2015) to demonstrate land cover change over time, mostly by human occupation in the region.

As seen earlier, the Cerrado region is home to a unique variety of vegetation physiognomies that would be hard to represent by an automated classification. The whole region's natural vegetation is composed by savannah structures with varying woodland density, and the transition between these zones would be very to capture by remote sensing measurements. A national initiative like MapBiomas or any other largescale land cover classification has, comprehensively, to simplify the classification system to achieve a broader view. For this reason, unlike other studies that consider a "typical Cerrado vegetation", herein we used the MapBiomas classes.

6.3.3. Remote sensing data

Landsat 5 and Landsat 8 scenes were used on WRS paths and rows presented in Figure 12. Landsat 5 scenes were taken from 1985 to 2011, whereas Landsat 8 scenes from 2013 to 2018. All scenes with less than 5% of cloud cover were collected. This, of course, led to a higher gathering through the region dry period (from May to October). Table 2 presents a more detailed view of the image collection used. We, then, computed two remote sensing indices to capture vegetation activity: Normalized Difference Vegetation Index (NDVI) and Normalized Difference Moisture Index (NDMI). The former to capture vegetation structure and the latter to capture leaf water content.

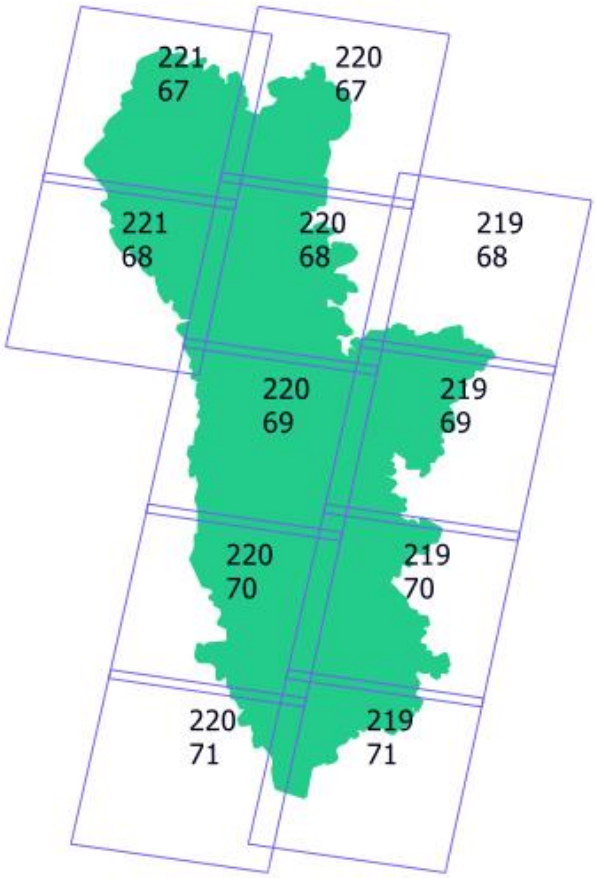

Figure 12: Landsat path-row coverage of the Urucuia Aquifer.

Path	Row	Jan	Feb	Mar	Apr	May	Jun	Jul	Aug	Sep	Oct	Nov	Dec
219	68	9	8	8	11	20	36	45	43	30	24	13	11
	69	7	4	7	11	24	31	44	35	30	21	11	12
	70	8	12	12	15	19	30	43	34	29	21	10	9
	71	10	7	12	19	19	30	36	34	26	18	8	7
220	67	5	3	1	6	23	38	38	40	36	15	10	7
	68	4	5	2	6	29	33	36	42	35	18	10	5
	69	4	5	5	7	26	32	36	38	35	15	9	5
	70	5	7	8	13	22	29	31	37	29	16	3	4
	71	8	7	7	13	26	23	28	35	27	15	2	5
221	67	2	4	3	7	11	40	46	42	21	9	5	5
	68	3	5	2	7	12	39	50	42	25	8	6	3
	Sum	65	67	67	115	231	361	433	422	323	180	87	73

Table 2: Imagery density by month.

6.4. Evapotranspiration (ET) estimation

The evapotranspiration (ET) was estimated for each scene using the surface energy balance algorithm for land (SEBAL) (Allen et al., 2011; Bastiaanssen et al., 1998a). The internal calibration was performed by an automated method proposed by Allen et al. (2013) with adjustments proposed by Kich et al. (2017). The algorithm was applied in the Google Earth Engine Platform (Gorelick et al., 2017), operated by the python API. Climate data were obtained from the Global Land Data Assimilation System (GLDAS), which integrates satellite-based and ground-based data sets for parameterizing, forcing and constraining land surface models (Qi et al., 2015).

6.5. Data analysis

We made two categories of analysis to capture groundwater controls in vegetation: in the contexts of land cover distribution and vegetation activity:

1. Land cover distribution: we separated HAND values by classes of 2% spatial frequency distribution, which gave 50 classes, presented in Figure 13. For each class, we computed the spatial occupation of the main land cover classes (Forest, Savanna, Grassland and Farmland) in each year with available classification (1985 to 2018).
2. Vegetation activity: we used HAND thresholds of $<5m$ riparian zone (RZ) and $>5m$ for upland zone (UZ) and the 4 most predominant land cover classes (Forest, Savanna, Grassland and Farmland) from the MapBiomas database that did not change over the whole period were used combined, generating 8 classes, for each 1000 pixels were randomly selected. In each pixel, then, we extracted NDVI and NDMI values and ET estimations from SEBAL.

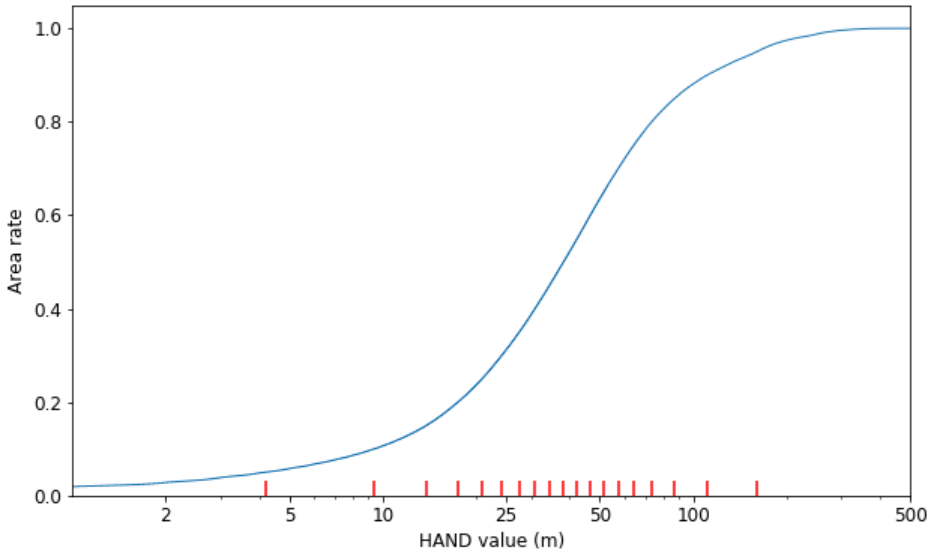

Figure 13: HAND values cumulative frequency distribution on study site. Red lines indicate 2% percentiles.

7. Results and discussion

7.1. Computed drainage network and HAND buffer for RZ

A comparison of drainage defined by different DATs and the vDAT method developed herein is presented in Figure 14. Using traditional GIS methods, we tested several DAT values, and drainage maps with the best performance were produced using single DATs of 5km² and 50km². The former with better representation on valleys' headwaters and the latter on the flat-topped mountain ranges ("chapadas"). In these plain mountain tops, however, one can find considerable big draining areas with no apparent drainage (some bigger than 500km²), making it very hard to not overestimate drainage on those areas. Even manually separating the "chapadas" from the rest of the landscape, it would very difficult to produce a drainage map using a single value of DAT. In valley bottoms, it was possible to have a reasonable map using the 5km² DAT, albeit missing a few headwaters in steeper and/or wetter areas – which indicates that a region with more variability in climate and topography would present an extra challenge.

The single DAT method can work very well in areas with homogeneous topography or when the representation of only the main rivers is sufficient. However, when drainage definition must be accurate, drainage definition should take into account other features rather than just a single DAT, and the TPI showed great potential in achieving that. As climate and geologic domain of the region studied here are relatively homogeneous, the only varying feature governing draining area for channel initiation would be topography. Using only the SRTM DEM as input we could achieve a well-suited drainage map for large-scale applications, which could capture varying DATs of the study site.

The vDAT method developed herein had definitely the best performance among all other traditional GIS methods. All macro features of terrain had a reasonably good drainage definition. It was possible to eliminate most of "false yes" drainages on the plain mountain tops and the "false no" on the steeper and wetter areas.

Once the channel is defined, computation of HAND is possible, and using a HAND threshold to buffer RZs was proven to be efficient. We tested different threshold HAND values bellow which

RZs would be better buffered. The HAND threshold with the best performance was 5m. Figure 15 presents the HAND buffer compared with satellite RGB image from Google.

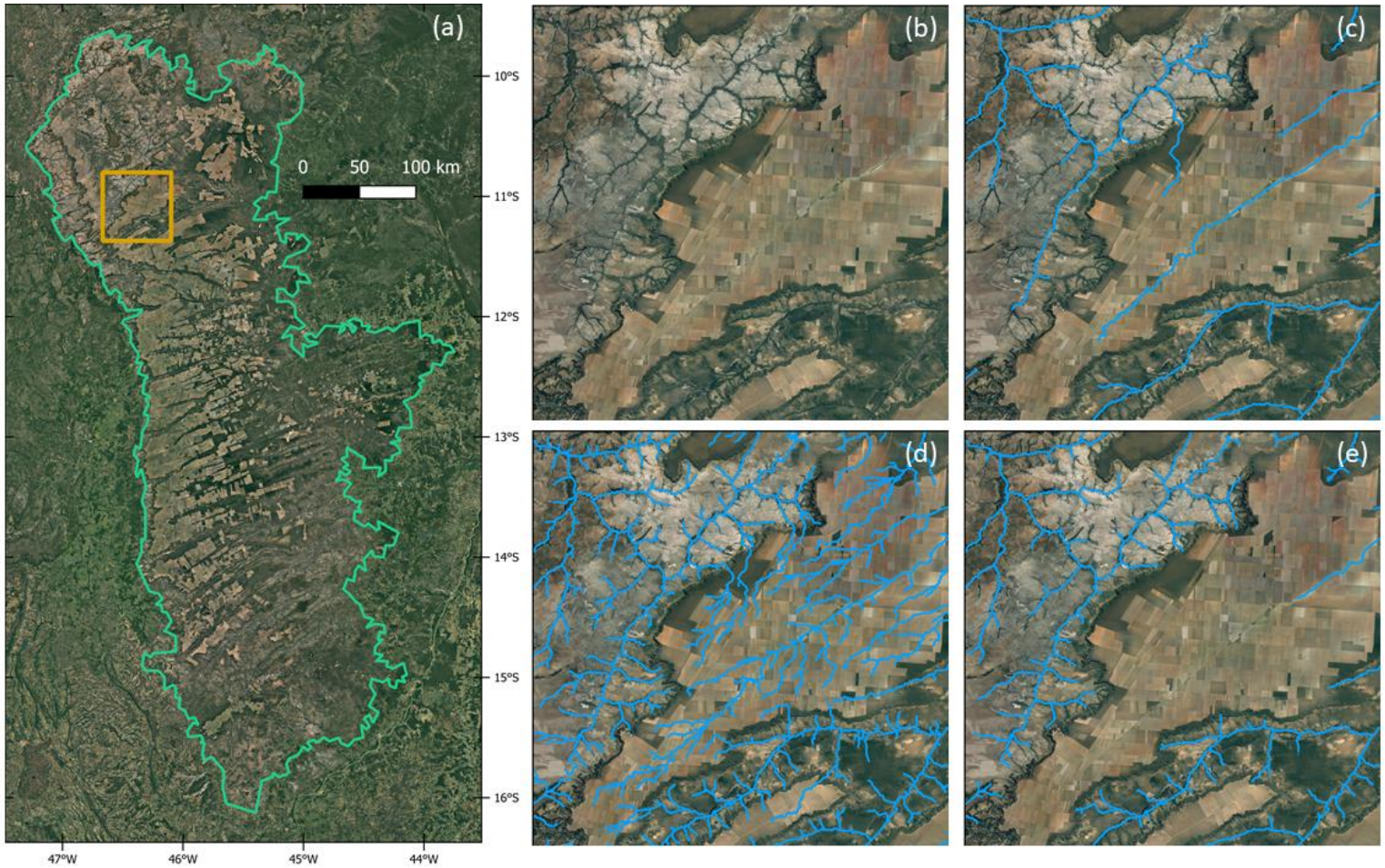

Figure 14: Satellite image provided by Google (a) of the study site (Urucuia aquifer), orange square represent zoom area (b) solely and with drainage density defined by (c) DAT of 500km², (d) DAT of 5km² and (e) using TPI criteria.

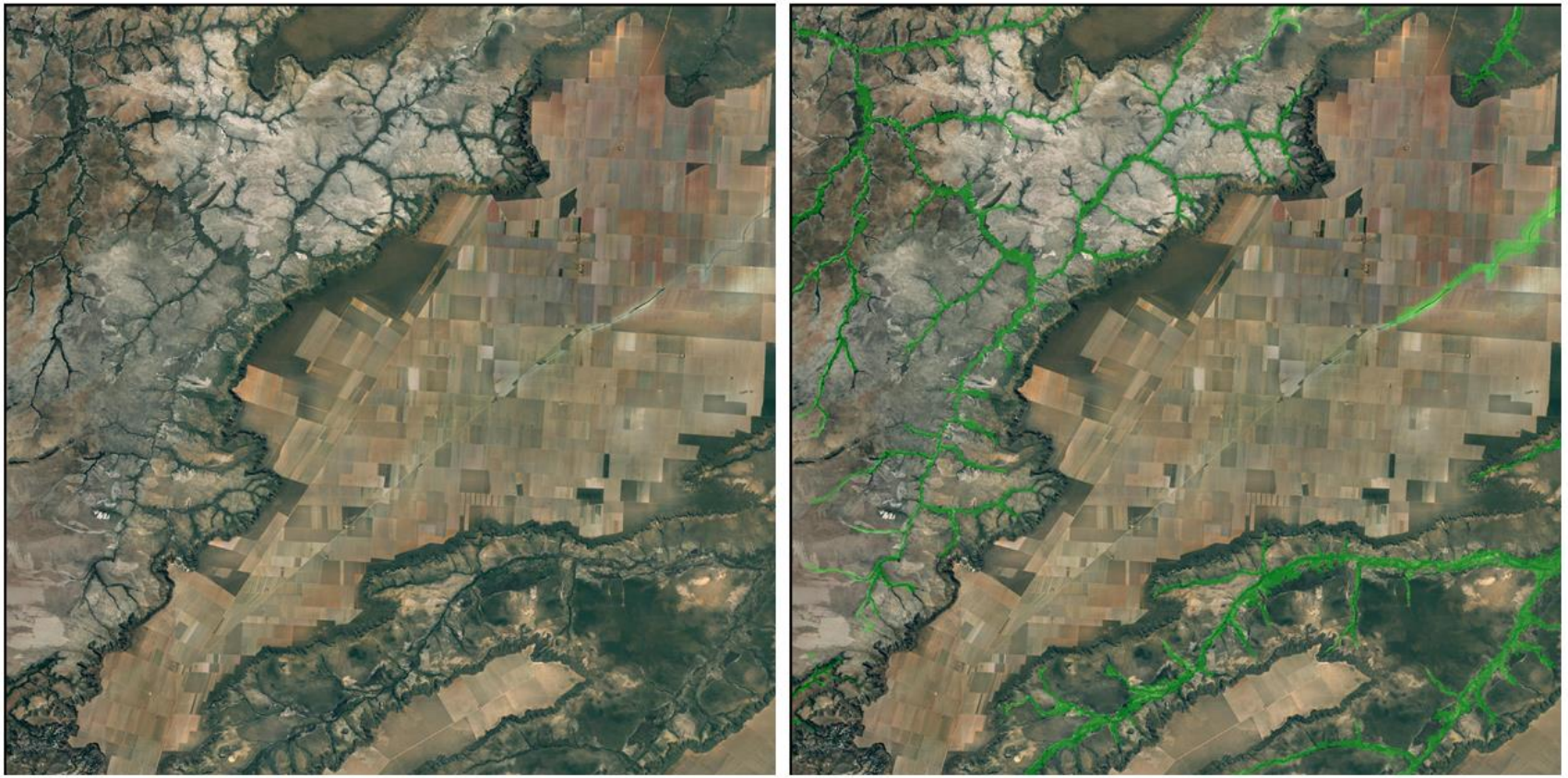

Figure 15: Same zoom area of previous image, showing riparian zone buffer defined by HAND < 5m.

7.2. HAND x Land cover distribution

The results of land cover distribution at HAND is presented in Figure 16. We chose 4 years to represent land cover change over the period. We could capture not only how natural vegetation is affected by water table, but also human activity. In the first years, Grasslands and Savannas occupied most part of the terrain (>80%) at all HAND classes and Farmlands only 7%. In recent years, land use changed dramatically with increasing demand for pastures and croplands. Farmlands represent now about 25% of the whole region, uplands being more affected (>40%). Forests seem to have greater occurrence in the RZ and at top HAND values – around 25%, while in the rest of the region the occupation is about 8%.

We could capture with HAND and MapBiomas land cover database how the classes of land cover are distributed over the Urucuia Aquifer System region. What really impressed here was that a pattern of historical human occupation was found, as it was expected that farmlands would have a more random distribution over HAND values. Even by visualization on satellite images that top mountain ranges ("chapadas") are experiencing more land use change in recent decades, a numerical relationship with HAND was a real surprise. An explanation for this pattern in occupation invoke again the concepts of landscape coevolution, as soil conditions imposed by long-term formation processes may have led to creating better farming conditions on the upland terrain portions.

As it was said here before, Cerrado vegetation presents many forms and distribution, being very hard to define with a large-scale classification such as the one used here. The classes of Savanna and Grassland are the most inaccurate as reported by MapBiomas (about 32% accuracy, while Forests and Farmlands have accuracies of 87% and 93% respectively). In these classes, there could be found Cerrado woodlands of varying densities, as well as mosaics of Forests, Grasslands and/or Farmlands. This may explain the occurrence of Savannas in shallow HAND values, where they were not expected to occur.

We could see that forests are naturally more present in very shallow and very deep HAND zones (around 25% while 8% in the remaining terrain portions). Typical Cerrado forests are expected to occur more densely in areas with deeper water tables, as they are known for their deep root systems and low tolerance to permanently wetted environments. Even so, they are surprisingly more

abundant in the farthest elevations from stream. Although classified the same way by the MapBiomas project, the mechanisms controlling their presence is different. Riparian Forests experience soils close to saturation (and sometimes waterlogged) all year round, while Upland Forests have greater variability in water uptake strategies (Rossatto et al., 2012).

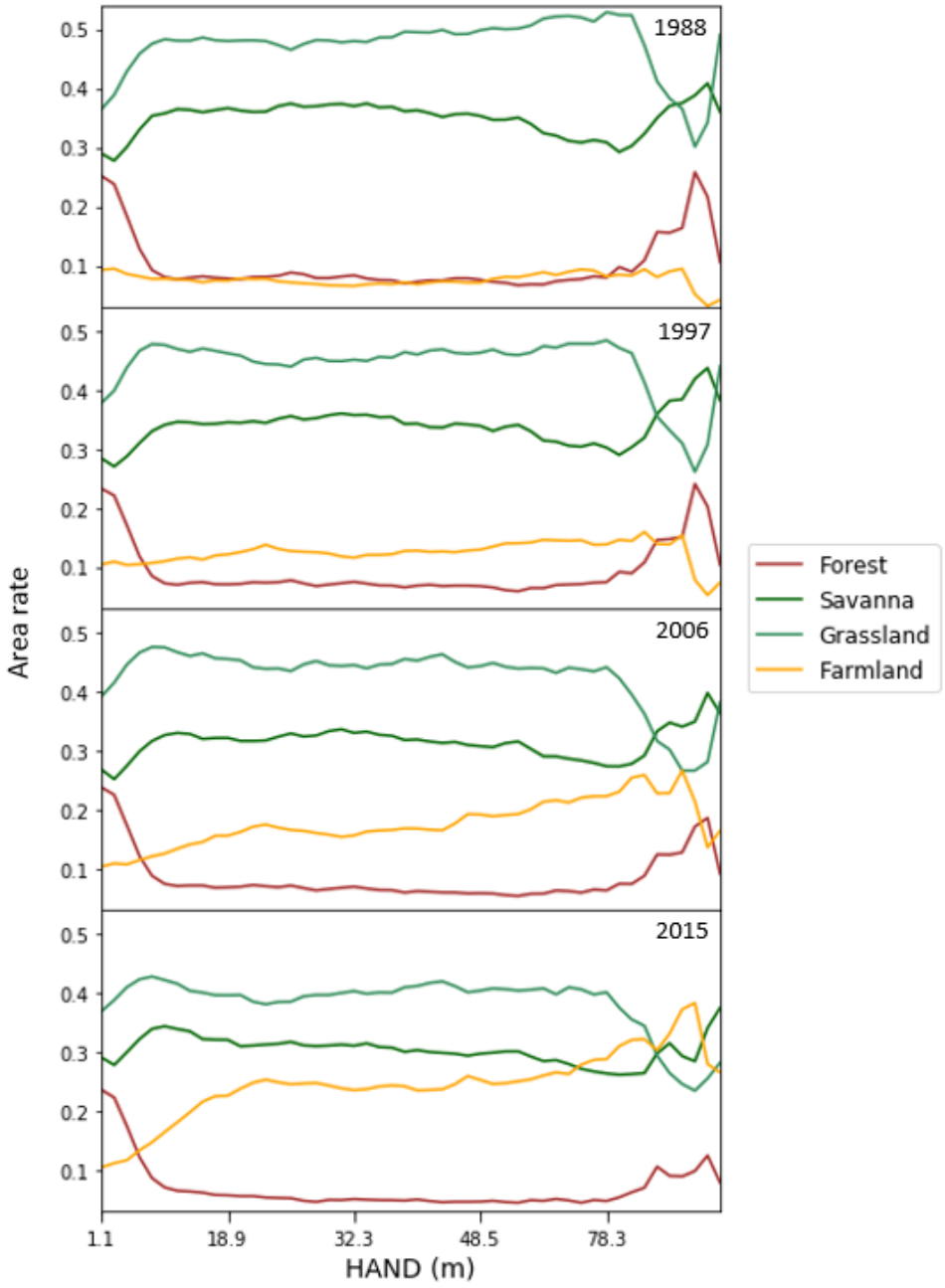

Figure 16: Land cover area rate for HAND classes in years 1988, 1997, 2006 and 2015.

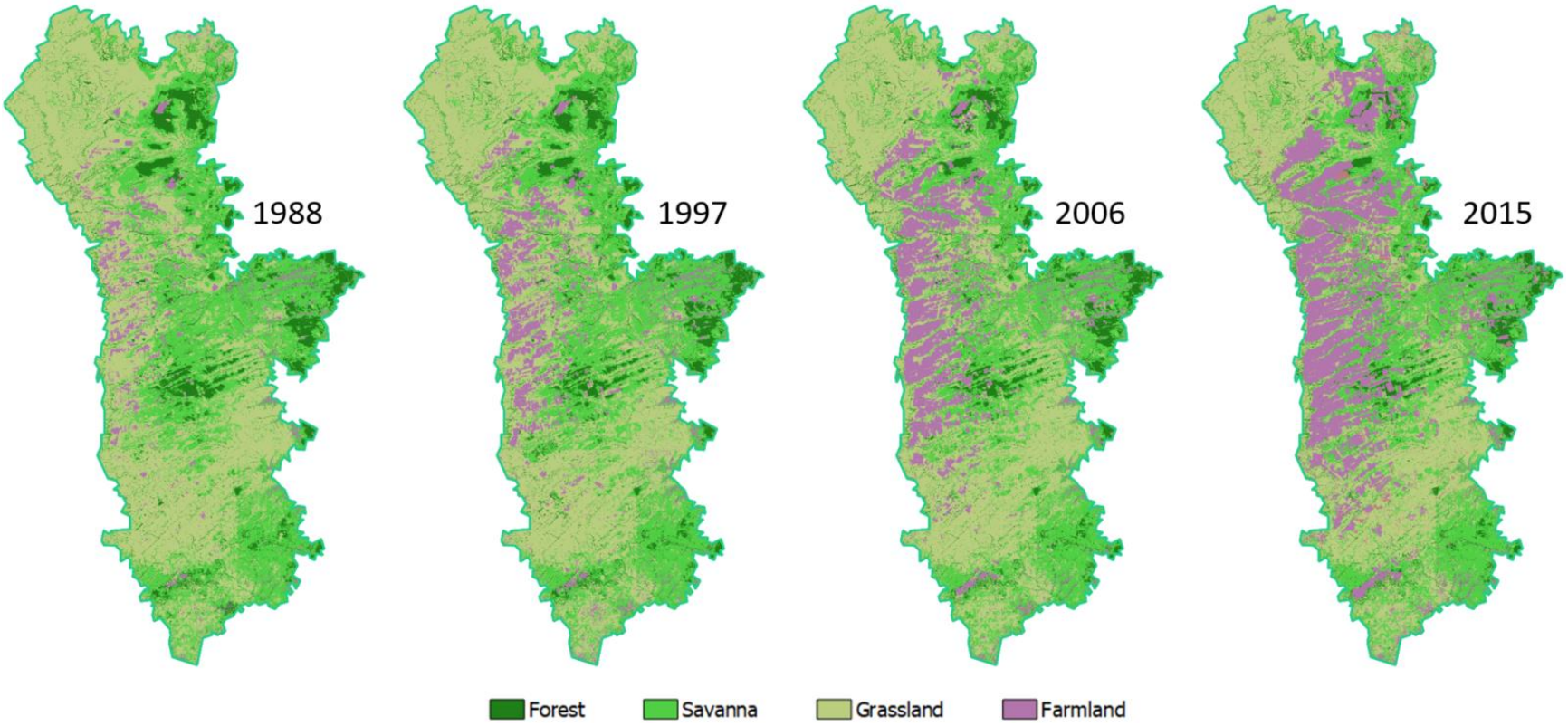

Figure 17: Land cover according to MapBiomas in representative area in years 1988, 1997, 2006 and 2015.

7.3. HAND x Vegetation activity

The following results are split into two subsections, one for the vegetation direct measurements (NDVI and NDMI) and one for ET estimation. The structure and figures of the subsections follow the same form. They are presented in two distinct time periods of 6 years (1986-1991 and 2013-2018), in forms of monthly averages and box-plots with three panels demonstrating distributions through (a) the whole time period, (b) the end of wet season (May) and (c) the end of dry season (September). These two periods were chosen in order to capture the contrast between wet and dry conditions. Between September and October, conditions are the driest in almost all Cerrado region, as it has experienced near 5 months with nearly no rain. Each figure structure is divided into Riparian and Upland zones for Forest, Savanna, Grassland and Farmland. At the end of this section, maps are presented to help on later discussion. Before going onto the subsections, annual averages of the 3 variables are presented next to see a general picture.

Figure 18 shows time series of annual averages through the period analysed. All three indicators of vegetation activity seem to be greater controlled by land cover class than by terrain position, Farmland being the land cover class which presented greatest difference between being on RZ or UZ. Savanna was the land cover class which presented the least difference in behaviour by terrain position. As for Grassland, there is a slight difference in values' magnitude across RZ and UZ that varies accordingly by the same amount in all three variables. Forest was the class that presented the most divergent behaviour, as it had a different pattern among all variables analysed. The terrain position showed a difference in NDVI values only in last years, in NDMI values throughout the whole period with greater difference in last years and in ET no significant difference was observed.

The grey area on the plots represent the periods which will be further looked into with more detail on next subsections. There are 3 main reasons for this split instead of taking the whole series: (1) data taken from 2013 to 2018 is from Landsat 8 mission, while the remaining data is from Landsat 5, which may lead to different values because band wave lengths are a little different between the two satellites; (2) the region is experiencing in recent years a warmer and drier climate, which may also lead to different behaviour in vegetation activity because water access may be greater in riparian zones across this period; and (3) land use changed considerably during the period, and although we only used pixels where land use did not change, still a bias can be present because of

interactions between landscape elements, mostly related to water use by croplands and pasture lands. Thus, the first and last 6 years of the analyses were chosen in order to take a considerable amount of data without disturbance on climate and land use change.

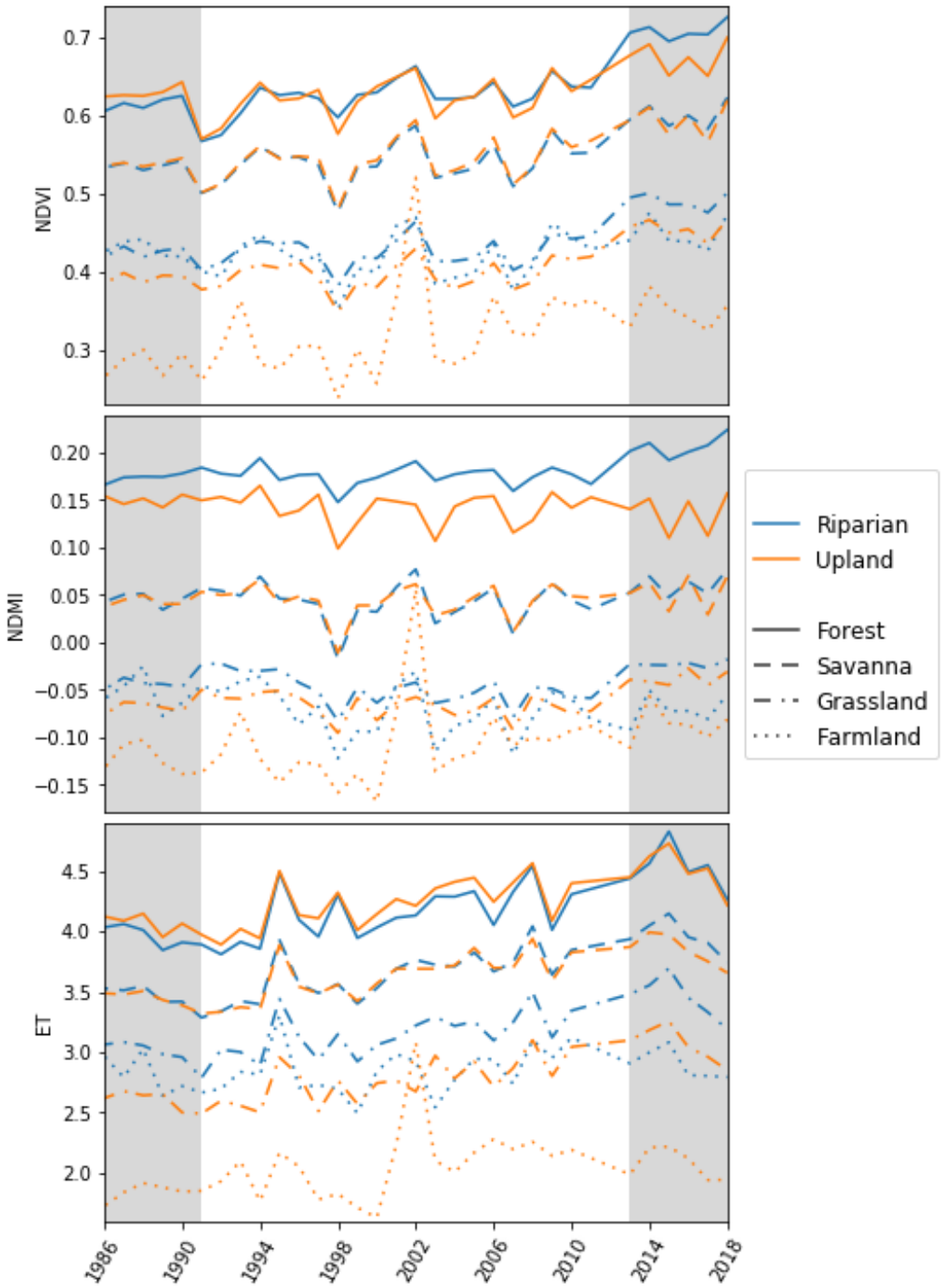

Figure 18: NDVI, NDMI and ET annual means for each terrain class and land cover type. Grey areas indicate periods further analyzed.

7.3.1. HAND x Vegetation indices

NDVI and NDMI values provide remote sensing direct measurements of vegetation activity, depending only on surface reflectance captured by the satellites. NDVI assess vegetation structure while NDMI assess leaf water content. Next comments will be regarding Figure 19 and Figure 20, which show monthly averages and box-plots at selected periods.

In terms of seasonality, all land cover classes in both terrain positions showed lower values at the end of dry season. Land cover class had a major control in the values, while terrain position influenced more the variation between the same land cover class. While NDVI values captured greater differences on Farmlands, NDMI values were more sensitive on Forests' behaviour.

Farmlands presented a wider distribution of values, as expected. While during the last period (2013-2018) they had no significant difference of NDMI measurements between RZ and UZ, NDVI captured a pronounced contrast, particularly at the dry season end, which in the RZ the average was greater than the UZ 3rd quartile. This indicates similar water contents between two zones with different leaf structures. The former could be explained by more irrigated croplands on UZ in recent years and the latter by the different crops that are favoured by soil conditions on different terrain portions. Of course, the Farmland land cover class presents a great variance of land use, and it is beyond the scope of this study to infer detailed information on it.

For both indices, the Savanna class did not present any meaningful difference for being whether on RZ or UZ. As for Grasslands, although distribution and seasonality followed the same behaviour, in RZ they presented a near constant difference in values. Overall classes and terrain portions during the earlier period, NDVI values were lower than later period, which may be intriguing because the last years were drier. NDMI values did not show significant magnitude differences between periods analysed, with exception of Riparian Forests, that showed greater values during the last period.

Forests' behaviour varied significantly between both the period of analysis and the indices used. NDMI showed a more pronounced difference than NDVI between wet and dry periods, as it is more sensitive in capturing water stress in plants. During the first 6-year period (1986-1991), no difference between terrain position was detected in NDVI and in NDMI a significant contrast was seen only at driest months. The latest period (2013-2018), on the other hand, revealed meaningful

variation between Forests in RZ and UZ at the end of the dry season for NDVI and at all seasons for NDMI. During this period in comparison with the first period, NDMI values in Forests were considerably greater in RZs and in UZs had a significant decrease during the dry season. As recent years had warmer and drier conditions than remaining period of analyses, this may explain why we observe that behaviour, as dry conditions would expect to limit water access in UZs and not in RZs.

It was not expected that Riparian Forests would suffer from water stress in the dry season, as they are in zones with high soil moisture. The NDVI and NDMI maps (Figure 21 and Figure 22) indicate that activity within these zones does not dimishes. By analyzing some points separately, it was noted similar or even greater values of the indices at the end of dry season, but this seems to be atenuated when plotting the whole data. This may be caused because, despite some narrow corridors continue to maintain high activity throughout the whole year, there are significant portions at the boundaries that do not. These portions are, still, classified as Forests by the MapBiomas. This can be seen by comparing the classification with the maps at the dry season end.

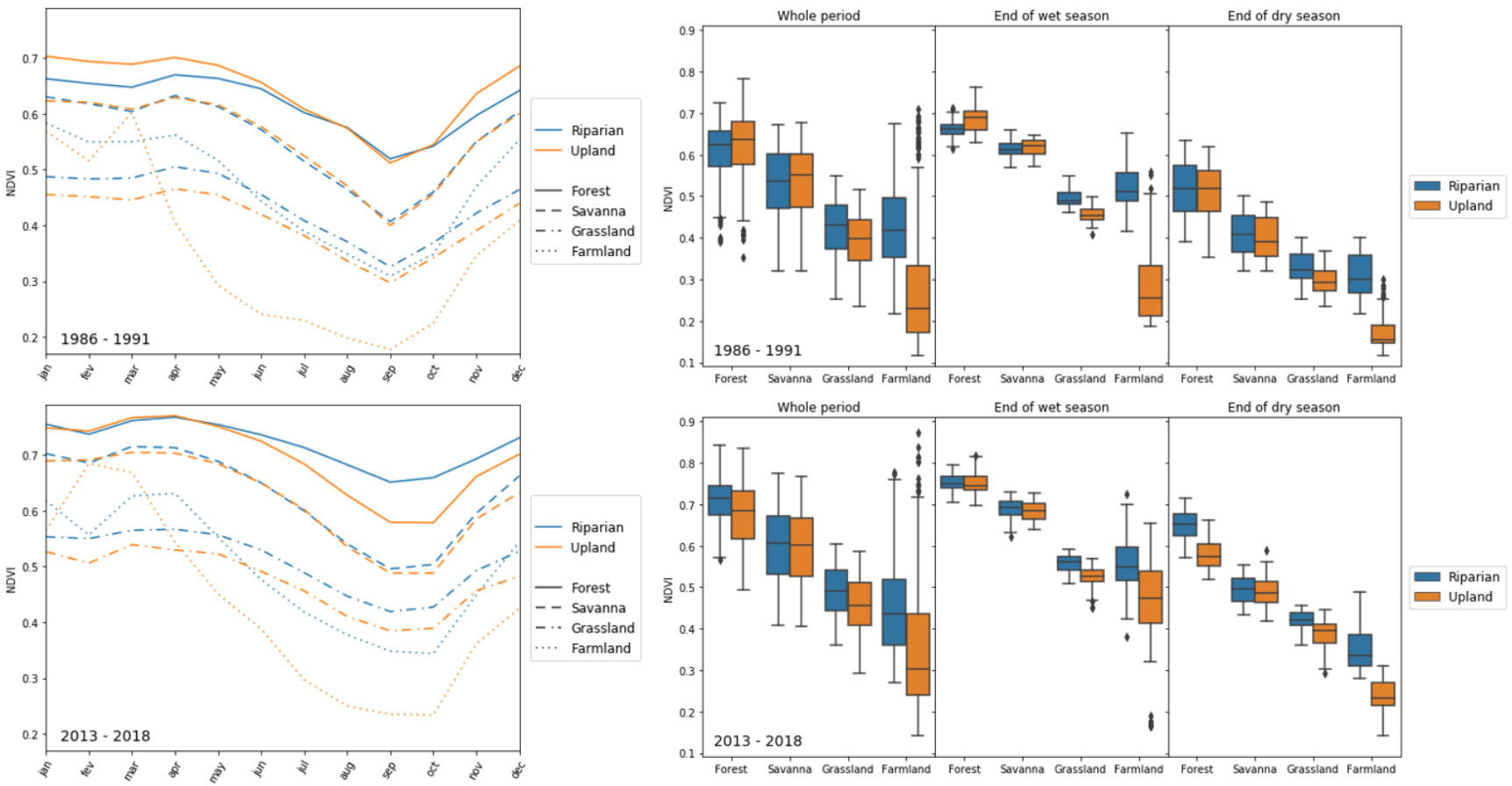

Figure 19: NDVI values in Riparian and Upland zones of land cover classes during 1986-1991 (upper) and 2013-2018 (bottom) – monthly averages (left) and box-plots (right) at whole period, end of wet season (May) and end of dry season (September)

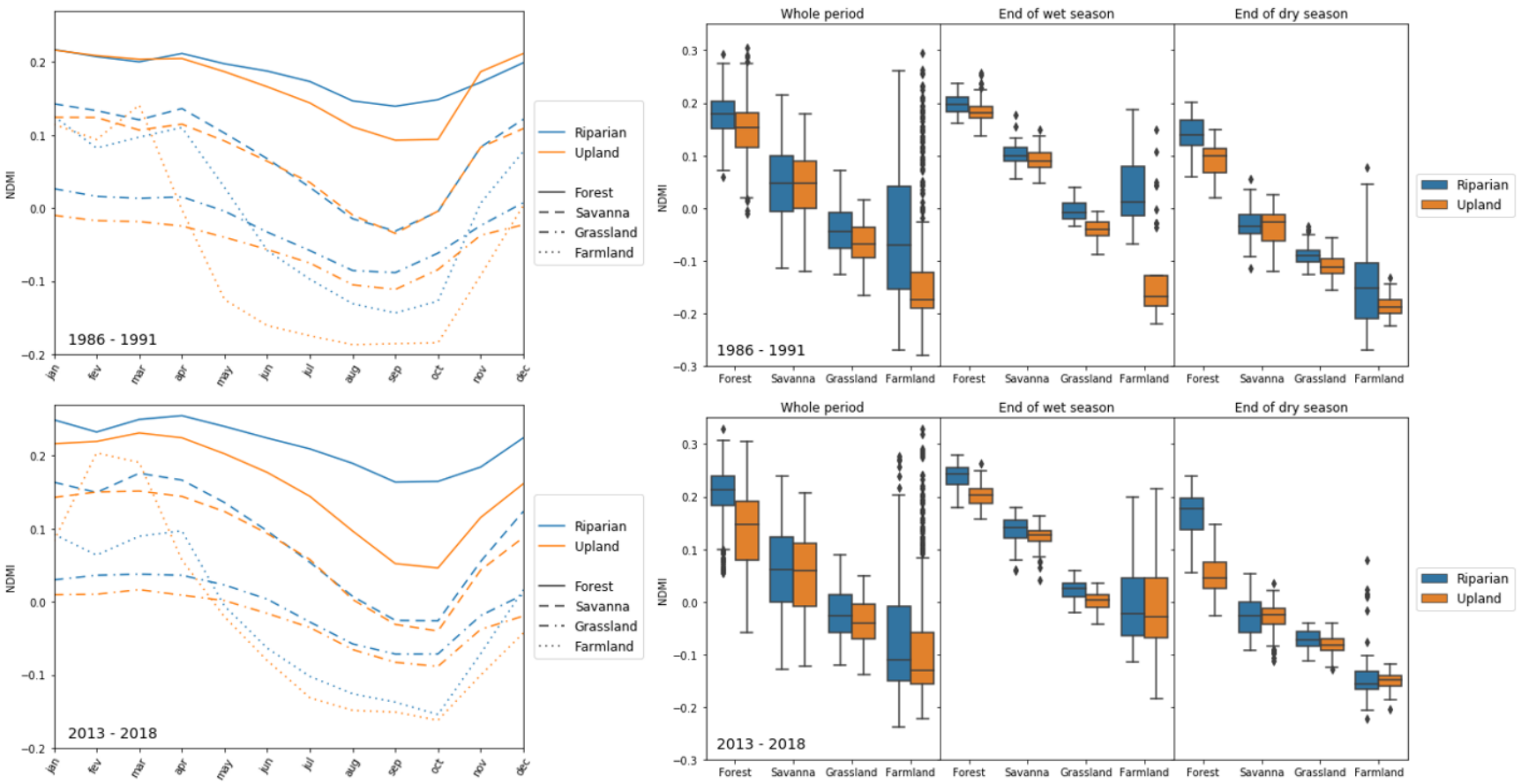

Figure 20: NDMI values in Riparian and Upland zones of land cover classes during 1986-1991 (upper) and 2013-2018 (bottom) – monthly averages (left) and box-plots (right) at whole period, end of wet season (May) and end of dry season (September).

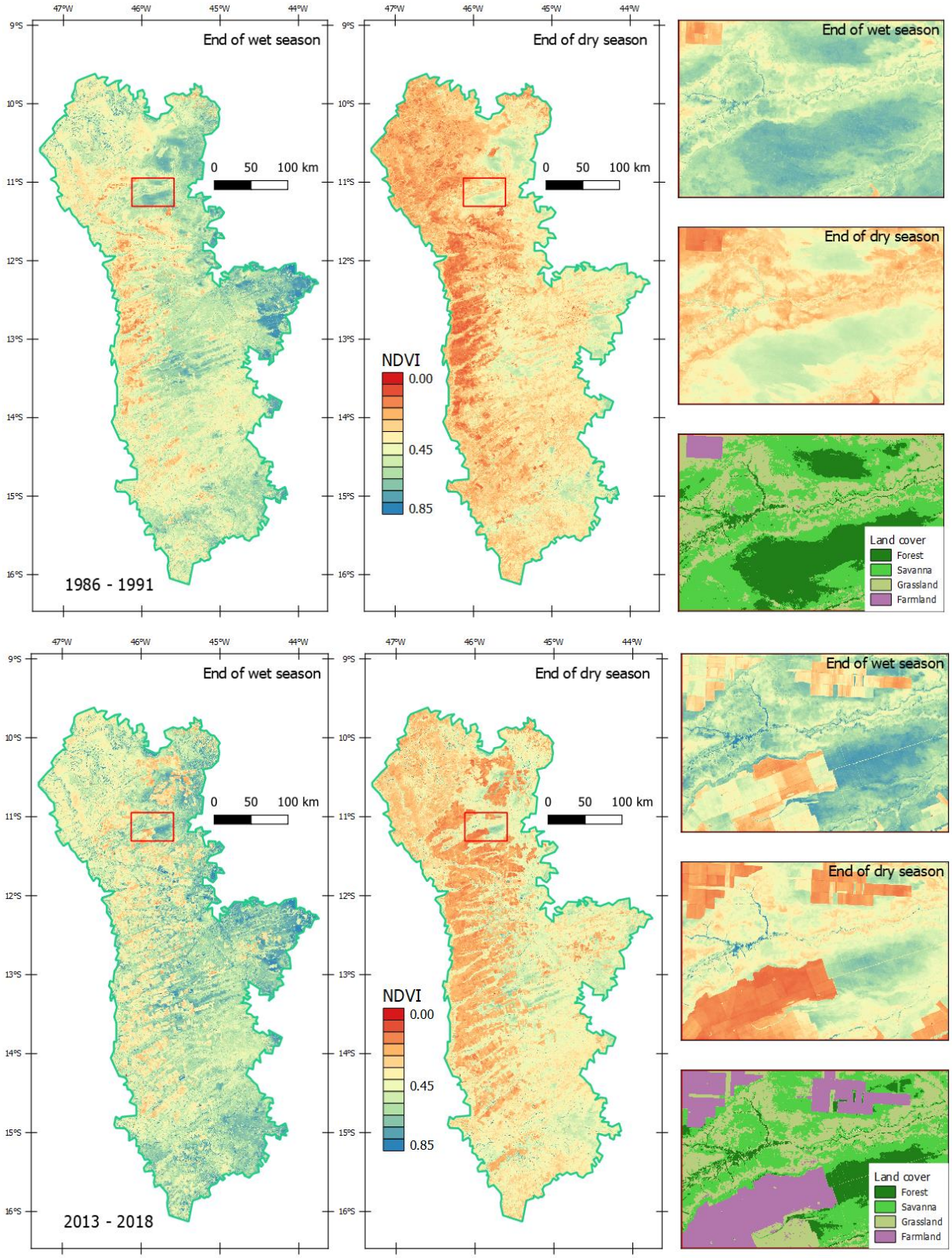

Figure 21: NDVI maps during 1986-1991 (upper) and 2013-2018 (bottom) in the Urucuia Aquifer System at the end of wet season and at the end of dry season. Rectangle indicates detailed area in the right, with MapBiomas land cover map of the period.

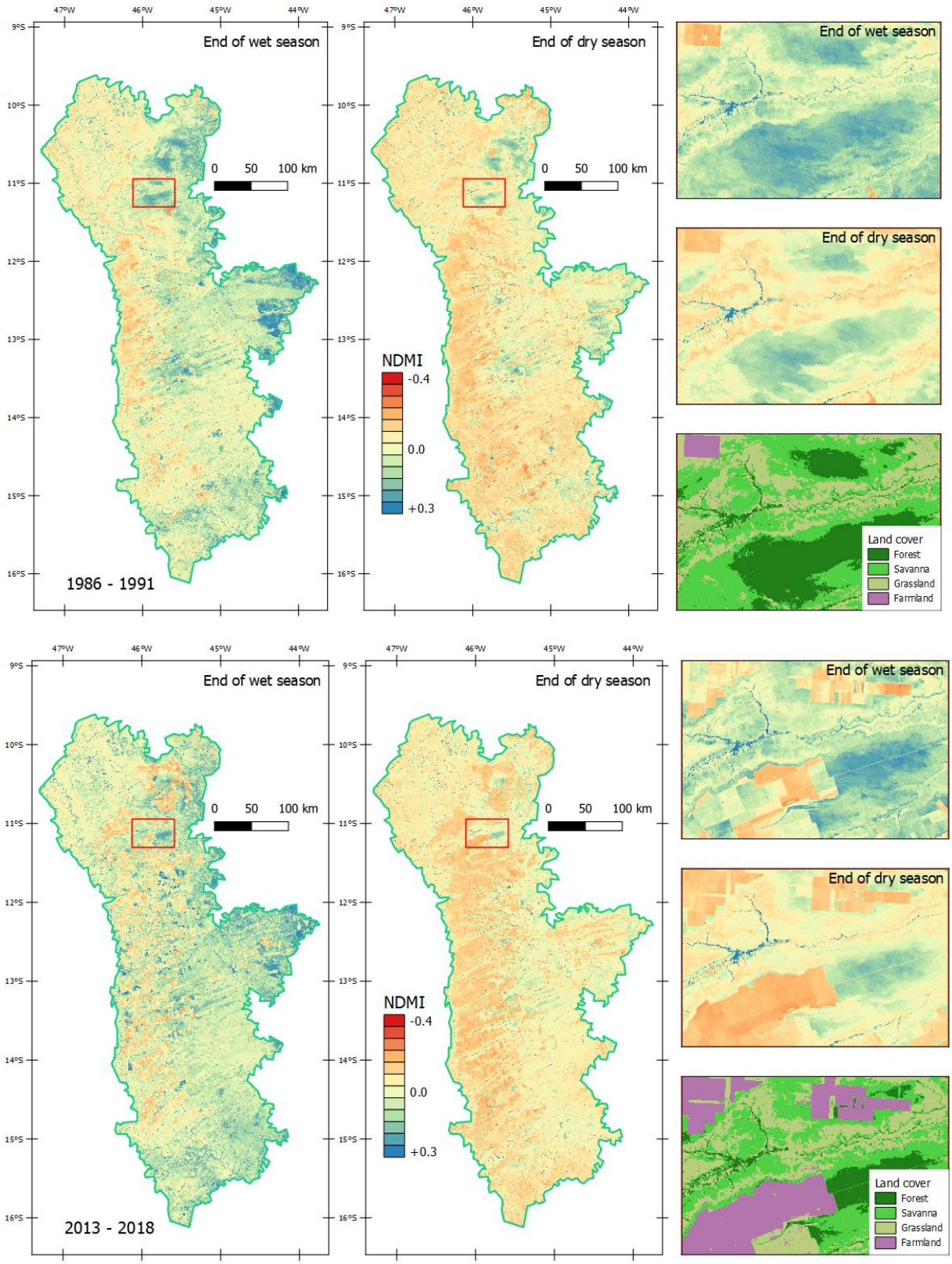

Figure 22: NDMI maps during 1986-1991 (upper) and 2013-2018 (bottom) in the Urucuia Aquifer System at the end of wet season and at the end of dry season. Rectangle indicates detailed area in the right, with MapBiomas land cover map of the period.

7.3.2. HAND x ET

The ET estimation with SEBAL model, as can be seen in Figure 23 and Figure 24, did not capture the seasonality in ET of vegetation activity computed by NDVI and NDMI. This was not expected to occur, as these measurements were used as a guide of vegetation activity, and it is presumed that ET would follow at the behaviour of these variables. What was really surprising was that ET was greater in the driest condition (September) than in the end of the wet season for natural vegetation (*i.e.* excluding farmlands). Moreover, ET seems to be overestimated by the model, particularly during the dry season, by comparison with other studies in the Cerrado region (Anache et al., 2018; Christoffersen et al., 2014; Giambelluca et al., 2009; Lima et al., 2001; Oliveira et al., 2014, 2015).

ET is a very hard variable to obtain, and its estimation by energy-balance methods, such as the SEBAL, requires calibration of parameter values (hot and cold pixel) and other constraints imposed by the operator regarding knowledge of energy balance and radiation physics (Allen et al., 2011), which were not made here in great effort. Also, the SEBAL model has been applied mostly for consumptive water use and agricultural crops (Liou and Kar, 2014) and calibration focus only on one vegetation type (*e.g.* Allen et al., 2011; Bastiaanssen et al., 1998b). For heterogeneous landscapes, which was the case here, more complex approaches should be considered (*e.g.* Chang et al., 2017; Gao et al., 2008). This may explain why only Farmlands and Grasslands had significant difference between RZ and UZ and why in Farmlands the seasonality is less “anomalous” comparing with vegetation measurements.

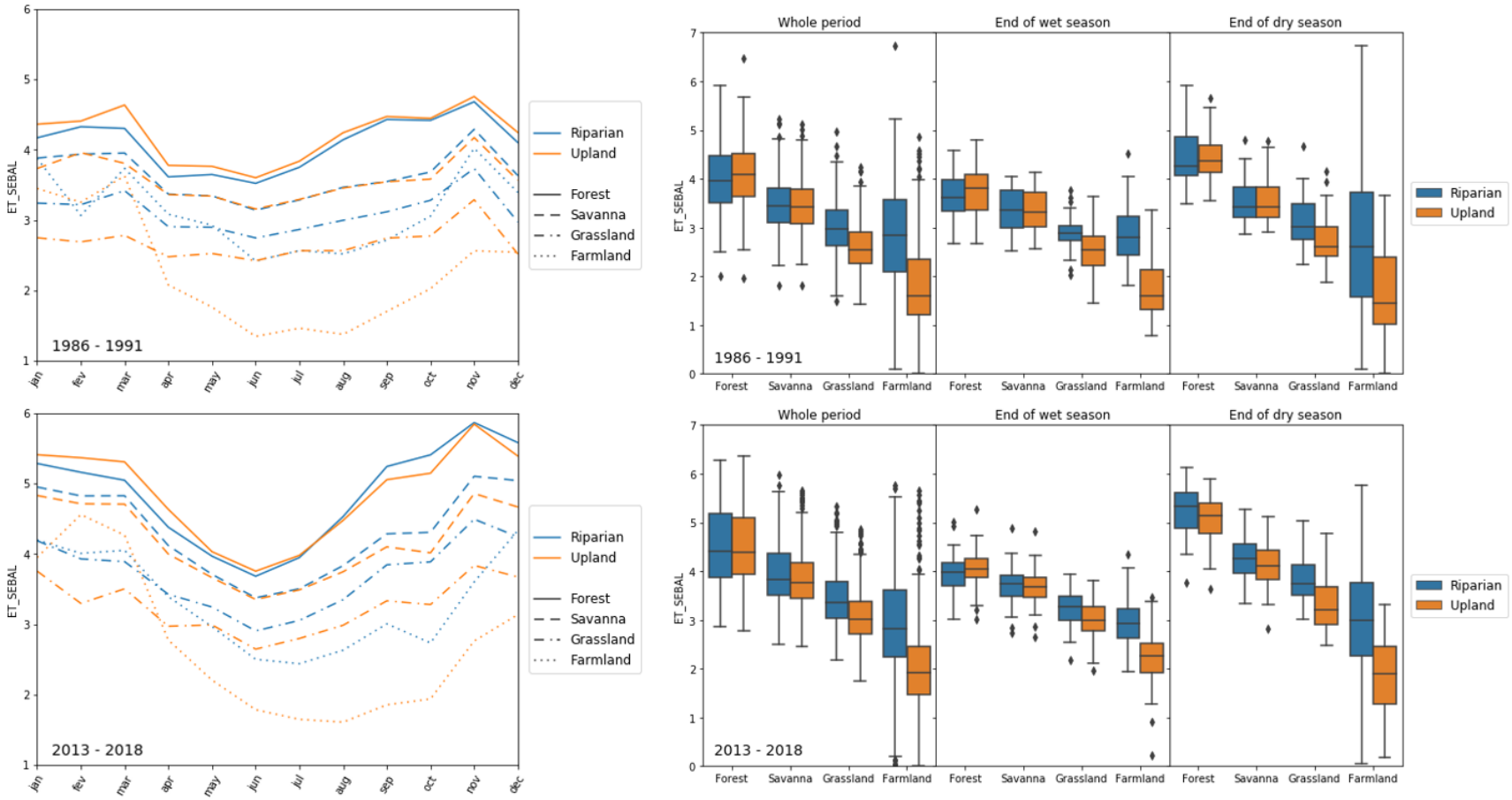

Figure 23: ET values in Riparian and Upland zones of land cover classes during 1986-1991 (upper) and 2013-2018 (bottom) – monthly averages (left) and box-plots (right) at whole period, end of wet season (May) and end of dry season (September).

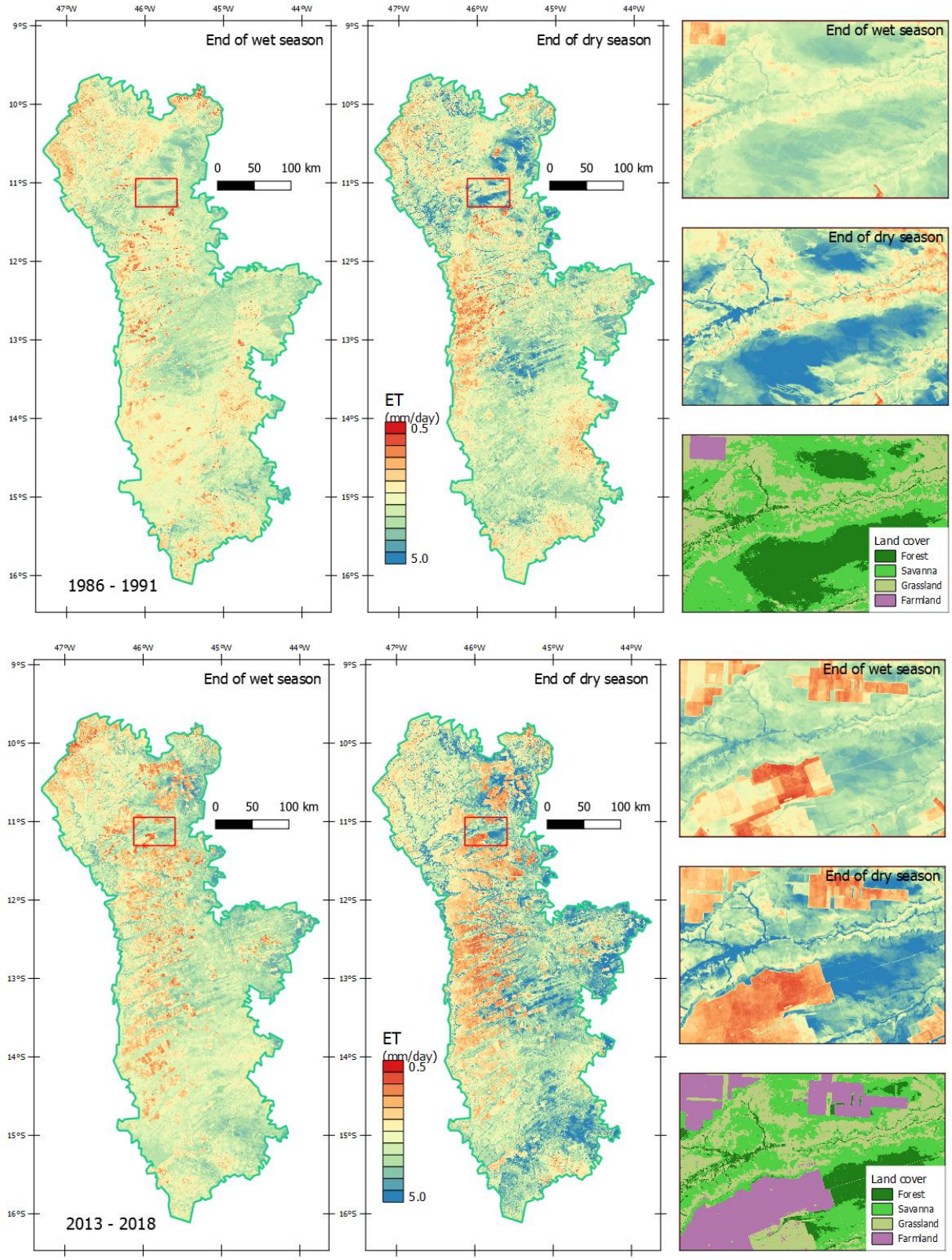

Figure 24: ET maps during 1986-1991 (upper) and 2013-2018 (bottom) in the Urucuia Aquifer System at the end of wet season and at the end of dry season. Rectangle indicates detailed area in the right, with MapBiomas land cover map of the period.

8. Conclusion

In this study, it was proposed to (1) identify RZs using topographic information and, from that, (2) investigate what differs between RZs and UZs in terms of vegetation behaviour and water access in the Brazilian Neo-Tropical Savanna (Cerrado). For the first objective, the height above nearest drainage (HAND) was used as a proxy for groundwater depth in a 140,000km² region (Urucuia aquifer) in the Brazilian Cerrado biome. Its computation was made with SRTM DEM using a drainage defined by a varying draining area threshold (vDAT) map made using the topographic position index (TPI). For the second objective, once a HAND map was achieved, it was evaluated against (a) historical MapBiomas land cover classification, (b) vegetation spectral indices (NDVI and NDMI) and evapotranspiration (ET) estimations using the surface energy balance algorithm for land (SEBAL). Landsat imagery from 1985 to 2018 was used to compute the spectral vegetation indices and the ET estimation.

Scientific contributions obtained herein came from what we could call a "Darwinian" approach, *i.e.*, by observing the system patterns as a whole and trying to understand what variables govern these patterns. We looked at the long-term aspects of landscape formation and remarked the possibility of accessing information by looking at relatively easy to obtain variables, such as topography and vegetation patterns. These aspects can be recognized as a sign of landscape coevolution, presented earlier in section 3.1. The innovative aspects of this study were:

1. the application of the topographic position index (TPI) alongside with slope and flow accumulations to determine drainage initiation, in means of obtaining a well-suited topographic index accounting hydrological similarity (HAND) and, thus, a RZ buffering; and
2. the usage of an index of hydrological similarity based on topography (HAND) alongside with a land cover yearly classification (MapBiomas) and historical remote sensing vegetation data (NDVI and NDMI) and ET estimations to capture landscape dynamics such as land cover distribution and vegetation behaviour in different landscape zones.

All applications that require an accurate drainage map may benefit from the vDAT method developed here. As drainage location indicates higher moisture conditions in the landscape, potential applications in the fields of geomorphology, hydrology and ecology are huge. A

particular case, which was used herein, was the computation of the height above nearest drainage (HAND).

The HAND map definition was essential in this study for the analysis made. We used the index as an indicator of soil moisture conditions shaped by topography, which proved to correlate well with land cover distribution and vegetation behaviour across different terrain zones. These moisture conditions may also lead to indications of landscape coevolution and hydrological similarity. The use of HAND was demonstrated to be promising, particularly in buffering RZs, as they follow drainage network and their water access is highly dependent on water table distance. We could capture with the HAND index and remote sensing measurements (1) how land cover is distributed across topographic gradients over the Urucuia region and (2) how vegetation activity differs between riparian zones (RZs) and upland zones (UZ).

Regarding land cover distribution, it was captured that forests in Cerrado naturally occur more densely in the extreme values of HAND (very shallow and very deep), although supported by different mechanisms (riparian forests by the shallow water table during all year and upland forests by deep rooted systems). Still, in all HAND classes the landscape is predominantly Savannas and Grasslands. In recent years, however, human agricultural expansion has been shifting the predominance of landscape towards farmlands, which now occupy around 25% of the Urucuia region. The historical occupation of farmlands in the region occur more in the upper portions of the terrain, possibly due to soil conditions stablished during landscape formation and evolution, which enable crops to thrive in these portions more than others.

As for vegetation activity, the land cover class seems to have more influence on vegetation behaviour than topographic position, for all indicators computed. Vegetation in the RZ suffer less from water stress than UZs, although in a small degree. his was seen most prominently through NDMI values in forests, which are greater in RZs than in UZs, particularly towards drier conditions, in terms of both seasonality (drier months) and inter-annual variability (drier years).

Despite this indication of more water available in RZs than UZs, the ET estimation could not capture these differences. Data from SEBAL model acquired in this study indicated ET overestimation towards drier conditions, which in turn caused mistaken seasonality. This could be caused by the methods used for parameter calibration that are mostly designed to assess information in croplands (specially irrigated). ET estimation in natural vegetation with high degree

of water stress is still a challenge and a gap to be filled by science. Future studies may provide the means to accurate assess plant water use differences between RZs and UZs at large scales.

9. References

Abbott, M.B., Bathurst, J.C., Cunge, J.A., O'Connell, P.E., and Rasmussen, J. (1986). An introduction to the European Hydrological System — Systeme Hydrologique Europeen, "SHE", 2: Structure of a physically-based, distributed modelling system. Journal of Hydrology *87*, 61–77.

Ågren, A.M., Lidberg, W., Strömgren, M., Ogilvie, J., and Arp, P.A. (2014). Evaluating digital terrain indices for soil wetness mapping – a Swedish case study. Hydrology and Earth System Sciences *18*, 3623–3634.

Allen, R., Irmak, A., Trezza, R., Hendrickx, J.M.H., Bastiaanssen, W., and Kjaersgaard, J. (2011). Satellite-based ET estimation in agriculture using SEBAL and METRIC. Hydrological Processes *25*, 4011–4027.

Allen, R.G., Burnett, B., Kramber, W., Huntington, J., Kjaersgaard, J., Kilic, A., Kelly, C., and Trezza, R. (2013). Automated Calibration of the METRIC-Landsat Evapotranspiration Process. JAWRA Journal of the American Water Resources Association *49*, 563–576.

Amorim Junior, V., and Lima, O.A.L. de (2007). Avaliação hidrogeológica do aqüífero Urucuia na bacia do rio das Fêmeas - BA usando resistividade e polarização elétrica induzida. Revista Brasileira de Geofísica *25*, 117–129.

Anache, J.A.A., Wendland, E., Rosalem, L.M.P., Youlton, C., and Oliveira, P.T.S. (2018). Hydrological trade-offs due to different land covers and land uses in the Brazilian Cerrado. Hydrology and Earth System Sciences Discussions 1–29.

Arnold, J.G., Allen, P.M., and Bernhardt, G. (1993). A comprehensive surface-groundwater flow model. Journal of Hydrology *142*, 47–69.

Baker, C., Lawrence, R., Montagne, C., and Patten, D. (2006). Mapping wetlands and riparian areas using Landsat ETM+ imagery and decision-tree-based models. Wetlands *26*, 465.

Bartels, S.F., Caners, R.T., Ogilvie, J., White, B., and Macdonald, S.E. (2018). Relating Bryophyte Assemblages to a Remotely Sensed Depth-to-Water Index in Boreal Forests. Front. Plant Sci. *9*.

Bastiaanssen, W.G.M., Menenti, M., Feddes, R.A., and Holtslag, A.A.M. (1998a). A remote sensing surface energy balance algorithm for land (SEBAL). 1. Formulation. Journal of Hydrology *212–213*, 198–212.

Bastiaanssen, W.G.M., Pelgrum, H., Wang, J., Ma, Y., Moreno, J.F., Roerink, G.J., and van der Wal, T. (1998b). A remote sensing surface energy balance algorithm for land (SEBAL).: Part 2: Validation. Journal of Hydrology *212–213*, 213–229.

Behrens, T., Zhu, A.-X., Schmidt, K., and Scholten, T. (2010). Multi-scale digital terrain analysis and feature selection for digital soil mapping. Geoderma *155*, 175–185.

Beven, K.J. (2012). Rainfall-Runoff Modelling: The Primer (John Wiley & Sons).

Beven, K.J., and Kirkby, M.J. (1979). A physically based, variable contributing area model of basin hydrology / Un modèle à base physique de zone d'appel variable de l'hydrologie du bassin versant. Hydrological Sciences Bulletin *24*, 43–69.

Blöschl, G., and Sivapalan, M. (1995). Scale issues in hydrological modelling: A review. Hydrological Processes *9*, 251–290.

Burrough, P.A., McDonnell, R.A., and Burrough, P.A. (1998). Principles of Geographical Information Systems (Oxford ; New York: Oxford University Press, USA).

Chang, Y., Ding, Y., Zhao, Q., and Zhang, S. (2017). Remote estimation of terrestrial evapotranspiration by Landsat 5 TM and the SEBAL model in cold and high-altitude regions: a case study of the upper reach of the Shule River Basin, China. Hydrological Processes *31*, 514–524.

Christoffersen, B.O., Restrepo-Coupe, N., Arain, M.A., Baker, I.T., Cestaro, B.P., Ciais, P., Fisher, J.B., Galbraith, D., Guan, X., Gulden, L., et al. (2014). Mechanisms of water supply and vegetation demand govern the seasonality and magnitude of evapotranspiration in Amazonia and Cerrado. Agricultural and Forest Meteorology *191*, 33–50.

Cole, M.M. (1960). Cerrado, Caatinga and Pantanal: The Distribution and Origin of the Savanna Vegetation of Brazil. The Geographical Journal *126*, 168–179.

Collischonn, W., Allasia, D., Da Silva, B.C., and Tucci, C.E.M. (2007). The MGB-IPH model for large-scale rainfall—runoff modelling. Hydrological Sciences Journal *52*, 878–895.

Crave, A., and Gascuel-Odoux, C. (1997). The Influence of Topography on Time and Space Distribution of Soil Surface Water Content. Hydrological Processes *11*, 203–210.

De Reu, J., Bourgeois, J., Bats, M., Zwertvaegher, A., Gelorini, V., De Smedt, P., Chu, W., Antrop, M., De Maeyer, P., Finke, P., et al. (2013). Application of the topographic position index to heterogeneous landscapes. Geomorphology *186*, 39–49.

Detty, J.M., and McGuire, K.J. (2010). Topographic controls on shallow groundwater dynamics: implications of hydrologic connectivity between hillslopes and riparian zones in a till mantled catchment. Hydrological Processes *24*, 2222–2236.

Dunne, T., and Black, R.D. (1970). Partial Area Contributions to Storm Runoff in a Small New England Watershed. Water Resources Research *6*, 1296–1311.

Eiten, G. (1972). The Cerrado Vegetation of Brazil. Botanical Review *38*, 201–341.

Famiglietti, J.S., Rudnicki, J.W., and Rodell, M. (1998). Variability in surface moisture content along a hillslope transect: Rattlesnake Hill, Texas. Journal of Hydrology *210*, 259–281.

Fan, Y. (2015). Groundwater in the Earth's critical zone: Relevance to large-scale patterns and processes. Water Resources Research *51*, 3052–3069.

Fan, Y., Miguez-Macho, G., Jobbágy, E.G., Jackson, R.B., and Otero-Casal, C. (2017). Hydrologic regulation of plant rooting depth. Proceedings of the National Academy of Sciences *114*, 10572–10577.

Flügel, W.-A. (1997). Combining GIS with regional hydrological modelling using hydrological response units (HRUs): An application from Germany. Mathematics and Computers in Simulation *43*, 297–304.

Furley, P.A. (1999). The nature and diversity of neotropical savanna vegetation with particular reference to the Brazilian cerrados. Global Ecology and Biogeography *8*, 223–241.

Gao, H., Sabo, J.L., Chen, X., Liu, Z., Yang, Z., Ren, Z., and Liu, M. (2018). Landscape heterogeneity and hydrological processes: a review of landscape-based hydrological models. Landscape Ecol *33*, 1461–1480.

Gao, Y., Long, D., and Li, Z.-L. (2008). Estimation of daily actual evapotranspiration from remotely sensed data under complex terrain over the upper Chao river basin in North China. International Journal of Remote Sensing *29*, 3295–3315.

Gharari, S., Hrachowitz, M., Fenicia, F., and Savenije, H.H.G. (2011). Hydrological landscape classification: investigating the performance of HAND based landscape classifications in a central European meso-scale catchment. Hydrology and Earth System Sciences *15*, 3275–3291.

Giambelluca, T.W., Scholz, F.G., Bucci, S.J., Meinzer, F.C., Goldstein, G., Hoffmann, W.A., Franco, A.C., and Buchert, M.P. (2009). Evapotranspiration and energy balance of Brazilian savannas with contrasting tree density. Agricultural and Forest Meteorology *149*, 1365–1376.

Gonçalves, R.D., Engelbrecht, B.Z., and Chang, H.K. (2018). Evolução da contribuição do Sistema Aquífero Urucuia para o Rio São Francisco, Brasil. R. Águas Subter. *32*, 1–10.

Gorelick, N., Hancher, M., Dixon, M., Ilyushchenko, S., Thau, D., and Moore, R. (2017). Google Earth Engine: Planetary-scale geospatial analysis for everyone. Remote Sensing of Environment *202*, 18–27.

Guisan, A., Weiss, S.B., and Weiss, A.D. (1999). GLM versus CCA spatial modeling of plant species distribution. Plant Ecology *143*, 107–122.

Hjerdt, K.N., McDonnell, J.J., Seibert, J., and Rodhe, A. (2004). A new topographic index to quantify downslope controls on local drainage. Water Resources Research *40*.

Howard, A.D. (1994). A detachment-limited model of drainage basin evolution. Water Resources Research *30*, 2261–2285.

Hubbert, M.K. (1940). The Theory of Ground-Water Motion. The Journal of Geology *48*, 785–944.

Hupp, C.R., and Osterkamp, W.R. (1996). Riparian vegetation and fluvial geomorphic processes. Geomorphology *14*, 277–295.

Jensen, J.R. (2006). Remote Sensing of the Environment: An Earth Resource Perspective (Upper Saddle River, NJ: Prentice Hall).

Kich, E. de M., Ruhoff, A., and Fleischmann, A.S. (2017). ESTIMATIVA AUTOMÁTICA DE EVAPOTRANSPIRAÇÃO POR SENSORIAMENTO REMOTO: INCERTEZAS E SENSIBILIDADE DO ALGORITMO SEBAL. 8.

Kollet, S.J., and Maxwell, R.M. (2006). Integrated surface–groundwater flow modeling: A free-surface overland flow boundary condition in a parallel groundwater flow model. Advances in Water Resources *29*, 945–958.

Kopecký, M., and Čížková, Š. (2010). Using topographic wetness index in vegetation ecology: does the algorithm matter? Applied Vegetation Science *13*, 450–459.

Kuglerová, L., Ågren, A., Jansson, R., and Laudon, H. (2014). Towards optimizing riparian buffer zones: Ecological and biogeochemical implications for forest management. Forest Ecology and Management *334*, 74–84.

Le Maitre, D.C., Scott, D.F., and Colvin, C. (1999). Review of information on interactions between vegetation and groundwater.

Leite, M.B., Xavier, R.O., Oliveira, P.T.S., Silva, F.K.G., and Matos, D.M.S. (2018). Groundwater depth as a constraint on the woody cover in a Neotropical Savanna. Plant Soil *426*, 1–15.

Lepsch, I.F. (2016). Formação e conservação dos solos (Oficina de Textos).

Lima, J.E.F.W., Silva, C.L. da, and Oliveira, C.A. da S. (2001). Comparação da evapotranspiração real simulada e observada em uma bacia hidrográfica em condições naturais de cerrado. Revista Brasileira de Engenharia Agrícola e Ambiental *5*, 33–41.

Lin, H., and Zhou, X. (2008). Evidence of subsurface preferential flow using soil hydrologic monitoring in the Shale Hills catchment. European Journal of Soil Science *59*, 34–49.

Liou, Y.-A., and Kar, S.K. (2014). Evapotranspiration Estimation with Remote Sensing and Various Surface Energy Balance Algorithms—A Review. Energies *7*, 2821–2849.

Lupon, A., Ledesma, J.L.J., and Bernal, S. (2018). Riparian evapotranspiration is essential to simulate streamflow dynamics and water budgets in a Mediterranean catchment. Hydrology and Earth System Sciences *22*, 4033–4045.

Maillard, P., Alencar-Silva, T., Clausi, D., Maillard, P., Alencar-Silva, T., and Clausi, D.A. (2008). An Evaluation of Radarsat-1 and ASTER Data for Mapping Veredas (Palm Swamps). Sensors *8*, 6055–6076.

Menduni, G., Pagani, A., Rulli, M.C., and Rosso, R. (2002). A non-conventional watershed partitioning method for semi-distributed hydrological modelling: the package ALADHYN. Hydrological Processes *16*, 277–291.

Miguez-Macho, G., and Fan, Y. (2012). The role of groundwater in the Amazon water cycle: 2. Influence on seasonal soil moisture and evapotranspiration. Journal of Geophysical Research: Atmospheres *117*.

Mokarram, M., Roshan, G., and Negahban, S. (2015). Landform classification using topography position index (case study: salt dome of Korsia-Darab plain, Iran). Model. Earth Syst. Environ. *1*, 40.

Montgomery, D.R., and Dietrich, W.E. (1988). Where do channels begin? Nature *336*, 232–234.

Montgomery, D.R., and Dietrich, W.E. (1989). Source areas, drainage density, and channel initiation. Water Resources Research *25*, 1907–1918.

Moore, I.D., Grayson, R.B., and Ladson, A.R. (1991). Digital terrain modelling: A review of hydrological, geomorphological, and biological applications. Hydrological Processes *5*, 3–30.

Mu, Q., Heinsch, F.A., Zhao, M., and Running, S.W. (2007). Development of a global evapotranspiration algorithm based on MODIS and global meteorology data. Remote Sensing of Environment *111*, 519–536.

Mu, Q., Zhao, M., and Running, S.W. (2011). Improvements to a MODIS global terrestrial evapotranspiration algorithm. Remote Sensing of Environment *115*, 1781–1800.

Murphy, P.N.C., Ogilvie, J., and Arp, P. (2009). Topographic modelling of soil moisture conditions: a comparison and verification of two models. European Journal of Soil Science *60*, 94–109.

Murphy, P.N.C., Ogilvie, J., Meng, F.-R., White, B., Bhatti, J.S., and Arp, P.A. (2011). Modelling and mapping topographic variations in forest soils at high resolution: A case study. Ecological Modelling *222*, 2314–2332.

Nobre, A.D., Cuartas, L.A., Hodnett, M., Rennó, C.D., Rodrigues, G., Silveira, A., Waterloo, M., and Saleska, S. (2011). Height Above the Nearest Drainage – a hydrologically relevant new terrain model. Journal of Hydrology *404*, 13–29.

O'Callaghan, J.F., and Mark, D.M. (1984). The extraction of drainage networks from digital elevation data. Computer Vision, Graphics, and Image Processing *28*, 323–344.

Oliveira, P.T.S., Nearing, M.A., Moran, M.S., Goodrich, D.C., Wendland, E., and Gupta, H.V. (2014). Trends in water balance components across the Brazilian Cerrado. Water Resources Research *50*, 7100–7114.

Oliveira, P.T.S., Wendland, E., Nearing, M.A., Scott, R.L., Rosolem, R., Rocha, D., and R, H. (2015). The water balance components of undisturbed tropical woodlands in the Brazilian cerrado. Hydrology and Earth System Sciences *19*, 2899–2910.

Oliveira, P.T.S., Leite, M.B., Mattos, T., Nearing, M.A., Scott, R.L., Xavier, R. de O., Matos, D.M. da S., and Wendland, E. (2017). Groundwater recharge decrease with increased vegetation density in the Brazilian cerrado. Ecohydrology *10*, e1759.

Oliveira-Filho, A.T.D., Shepherd, G.J., Martins, F.R., and Stubblebine, W.H. (1989). Environmental factors affecting physiognomic and floristic variation in an area of cerrado in central Brazil. Journal of Tropical Ecology *5*, 413–431.

Oltean, G.S., Comeau, P.G., and White, B. (2016). Linking the Depth-to-Water Topographic Index to Soil Moisture on Boreal Forest Sites in Alberta. For Sci *62*, 154–165.

Park, S.J., and van de Giesen, N. (2004). Soil–landscape delineation to define spatial sampling domains for hillslope hydrology. Journal of Hydrology *295*, 28–46.

Passalacqua, P., Trung, T.D., Foufoula-Georgiou, E., Sapiro, G., and Dietrich, W.E. (2010). A geometric framework for channel network extraction from lidar: Nonlinear diffusion and geodesic paths. Journal of Geophysical Research: Earth Surface *115*.

Pelletier, J.D., and Rasmussen, C. (2009). Geomorphically based predictive mapping of soil thickness in upland watersheds. Water Resources Research *45*.

Purkis, S.J., and Klemas, V.V. (2011). Remote Sensing and Global Environmental Change (Chichester, West Sussex, UK ; Hoboken, N.J: Wiley-Blackwell).

Qi, W., Zhang, C., Fu, G., and Zhou, H. (2015). Global Land Data Assimilation System data assessment using a distributed biosphere hydrological model. Journal of Hydrology *528*, 652–667.

Ratter, J.A., Ribeiro, J.F., and Bridgewater, S. (1997). The Brazilian Cerrado Vegetation and Threats to its Biodiversity. Annals of Botany *80*, 223–230.

Rennó, C.D., Nobre, A.D., Cuartas, L.A., Soares, J.V., Hodnett, M.G., Tomasella, J., and Waterloo, M.J. (2008). HAND, a new terrain descriptor using SRTM-DEM: Mapping terra-firme rainforest environments in Amazonia. Remote Sensing of Environment *112*, 3469–3481.

Riley, J.W., Calhoun, D.L., Barichivich, W.J., and Walls, S.C. (2017). Identifying Small Depressional Wetlands and Using a Topographic Position Index to Infer Hydroperiod Regimes for Pond-Breeding Amphibians. Wetlands *37*, 325–338.

Rossatto, D.R., de Carvalho Ramos Silva, L., Villalobos-Vega, R., Sternberg, L. da S.L., and Franco, A.C. (2012). Depth of water uptake in woody plants relates to groundwater level and vegetation structure along a topographic gradient in a neotropical savanna. Environmental and Experimental Botany *77*, 259–266.

Rossatto, D.R., Silva, L.C.R., Sternberg, L.S.L., and Franco, A.C. (2014). Do woody and herbaceous species compete for soil water across topographic gradients? Evidence for niche partitioning in a Neotropical savanna. South African Journal of Botany *91*, 14–18.

Savenije, H.H.G. (2010). *HESS Opinions* "Topography driven conceptual modelling (FLEX-Topo)." Hydrology and Earth System Sciences *14*, 2681–2692.

Schietti, J., Emilio, T., Rennó, C.D., Drucker, D.P., Costa, F.R.C., Nogueira, A., Baccaro, F.B., Figueiredo, F., Castilho, C.V., Kinupp, V., et al. (2014). Vertical distance from drainage drives floristic composition changes in an Amazonian rainforest. Plant Ecology & Diversity *7*, 241–253.

Scott, R.L., Cable, W.L., Huxman, T.E., Nagler, P.L., Hernandez, M., and Goodrich, D.C. (2008). Multiyear riparian evapotranspiration and groundwater use for a semiarid watershed. Journal of Arid Environments *72*, 1232–1246.

Scott, R.L., Huxman, T.E., Barron-Gafford, G.A., Jenerette, G.D., Young, J.M., and Hamerlynck, E.P. (2014). When vegetation change alters ecosystem water availability. Global Change Biology *20*, 2198–2210.

Serrat-Capdevila, A., Scott, R.L., James Shuttleworth, W., and Valdés, J.B. (2011). Estimating evapotranspiration under warmer climates: Insights from a semi-arid riparian system. Journal of Hydrology *399*, 1–11.

Sivapalan, M., and Blöschl, G. (2015). Time scale interactions and the coevolution of humans and water. Water Resources Research *51*, 6988–7022.

Sørensen, R., Zinko, U., and Seibert, J. (2006). On the calculation of the topographic wetness index: evaluation of different methods based on field observations. Hydrology and Earth System Sciences Discussions *10*, 101–112.

Stromberg, J.C., Tiller, R., and Richter, B. (1996). Effects of Groundwater Decline on Riparian Vegetation of Semiarid Regions: The San Pedro, Arizona. Ecological Applications *6*, 113–131.

Tabacchi, E., Lambs, L., Guilloy, H., Planty-Tabacchi, A.-M., Muller, E., and Décamps, H. (2000). Impacts of riparian vegetation on hydrological processes. Hydrological Processes *14*, 2959–2976.

Tagil, S., and Jenness, J. (2008). GIS-Based Automated Landform Classification and Topographic, Landcover and Geologic Attributes of Landforms Around the Yazoren Polje, Turkey - SciAlert Responsive Version. Journal of Aplied Sciences *8*, 910–921.

Tarboton, D.G. (1997). A new method for the determination of flow directions and upslope areas in grid digital elevation models. Water Resources Research *33*, 309–319.

Tarboton, D.G., and Ames, D.P. (2001). Advances in the Mapping of Flow Networks from Digital Elevation Data. World Water and Environmental Resources Congress 1–10.

Troch, P.A., Carrillo, G., Sivapalan, M., Wagener, T., and Sawicz, K. (2013). Climate-vegetation-soil interactions and long-term hydrologic partitioning: signatures of catchment co-evolution. Hydrology and Earth System Sciences *17*, 2209–2217.

Troch, P.A., Lahmers, T., Meira, A., Mukherjee, R., Pedersen, J.W., Roy, T., and Valdés-Pineda, R. (2015). Catchment coevolution: A useful framework for improving predictions of hydrological change? Water Resources Research *51*, 4903–4922.

Villalobos-Vega, R., Salazar, A., Miralles-Wilhelm, F., Haridasan, M., Franco, A.C., and Goldstein, G. (2014). Do groundwater dynamics drive spatial patterns of tree density and diversity in Neotropical savannas? Journal of Vegetation Science *25*, 1465–1473.

Weiss, A. (2001). Topographic position and landforms analysis (San Diego, CA).

White, B., Ogilvie, J., Campbell, D.M.H.M.H., Hiltz, D., Gauthier, B., Chisholm, H.K.H., Wen, H.K., Murphy, P.N.C.N.C., and Arp, P.A.A. (2012). Using the Cartographic Depth-to-Water Index to Locate Small Streams and Associated Wet Areas across Landscapes. Canadian Water Resources Journal / Revue Canadienne Des Ressources Hydriques *37*, 333–347.

Wilson, J.P., and Gallant, J.C. (2000). Terrain Analysis: Principles and Applications (John Wiley & Sons).

Yamazaki, D., Ikeshima, D., Tawatari, R., Yamaguchi, T., O'Loughlin, F., Neal, J.C., Sampson, C.C., Kanae, S., and Bates, P.D. (2017). A high-accuracy map of global terrain elevations. Geophysical Research Letters *44*, 5844–5853.

Yamazaki, D., Ikeshima, D., Sosa, J., Bates, P.D., Allen, G.H., and Pavelsky, T.M. (2019). MERIT Hydro: A High-Resolution Global Hydrography Map Based on Latest Topography Dataset. Water Resources Research *55*, 5053–5073.